Noname manuscript No.
(will be inserted by the editor)

Optimized Schwarz methods with elliptical domain decompositions

Xin Chen · Martin J. Gander · Yingxiang Xu

Received: date / Accepted: date

Abstract Over the past decade, partial differential equation models in elliptical geometries have become a focus of interest in several scientific and engineering applications: the classical studies of flow past a cylinder, the spherical particles in nano-fluids and spherical water filled domains are replaced by elliptical geometries which more accurately describe a wider class of physical problems of interest. Optimized Schwarz methods (OSMs) are among the best parallel methods for such models. We study here for the first time OSMs with elliptical domain decompositions, i.e. decompositions into an ellipse and elliptical rings. Using the technique of separation of variables, we decouple the spatial variables and reduce the subdomain problems to radial Mathieu like equations defined on finite intervals, which allows us to derive and study a new family of OSMs. Our analysis reveals that the optimized transmission parameters are not constants any more along the elliptical interfaces. We can prove however also that using the constant optimized parameters from the straight interface analysis in the literature scaled locally by the interface curvature is still efficient in an asymptotic sense, which leads to the important discovery of a unique factor in the optimized parameters and asymptotic performance determined by the geometry of the decomposition. We use numerical examples to illustrate our analysis and findings.

Partially supported by NSFC-12071069, 11671074 and the Fundamental Research Funds for the Central Universities (No. 2412020XK001).

X. Chen
School of Mathematics and Statistics, Northeast Normal University, Changchun 130024, China. E-mail: 1336176626@qq.com

M. J. Gander
Section de Mathématiques, Université de Genève, 2-4 rue du Lièvre, CP 64, CH-1211, Genève, Suisse. E-mail: Martin.Gander@unige.ch

Y. Xu
Corresponding author. School of Mathematics and Statistics, Northeast Normal University, Changchun 130024, China. E-mail: yxxu@nenu.edu.cn

Keywords optimized Schwarz method · elliptical domain decomposition · optimized transmission condition · curved interfaces

1 Introduction

We consider the (negative) definite screened Laplace model problem

$$(\Delta - \eta)u = g, \quad \eta > 0, \tag{1}$$

on a bounded domain $\Omega \subset \mathbb{R}^2$, together with a boundary condition $\mathcal{B}u|_{\partial\Omega} = 0$ such that the problem (1) is well posed. The model problem (1) is also known in the literature as the Helmholtz equation with the good sign [49], the modified Helmholtz equation, see e.g. [4], or simply the positive definite Helmholtz equation, and its properties are very different from the ones of the true Helmholtz equation studied by Helmholtz himself [33,19], which is indefinite with $\eta := -k^2 < 0$ where k denotes the wave number [15]. Partial differential equation models like (1) in domains with elliptically shaped boundary have a strong background in physical applications, see for example the recent literature [14, 40,41] for analysis on fluid flow; [42,45] for heat transfer in fluid flow; [2] for heat transfer from a moving elliptical cylinder, where the model parameter η in (1) is related to the thermal diffusivity of the material and the moving speed of the heat source; [3,4] for groundwater flow, where the quantity $\sqrt{\eta}$ corresponds to the leakage factor; and also [35,39] for wave scattering problems. Computational efforts have been made in [36], where a fast Poisson solver was developed for elliptical domains using a truncated Fourier series. Recently, spectral approximations for both Helmholtz and positive definite Helmholtz problems using Mathieu functions were introduced and analyzed in [46]. There are however, to our best knowledge, no results yet for domain decomposition methods on such an elliptical geometry, which is the first motivation for our present research. The second motivation is to better understand the influence of subdomain geometry on the performance of optimized Schwarz methods (OSMs), which are known to be among the best modern domain decomposition methods because of their fast convergence due to optimized transmission conditions. OSMs have been successfully applied to many partial differential equations, including our model problem [16], Helmholtz problems [22,47,29] with an extensive review in [30], wave equations [23,20], Maxwell's equations [44,12,7,13], advection reaction diffusion problems [34,21,6,5], and shallow water equations [38,43]. In OSM analysis, the computational domain is usually assumed to be an infinite domain and a domain decomposition of two half planes is generally used, to be able to apply Fourier techniques to obtain and optimize the convergence factor in the frequency domain. However, in applications the subdomains are generally finite and the influence of geometry on the performance of the OSMs is a current field of active research. The first investigation in this direction was performed in [18], where optimized Robin transmission conditions for both Dirichlet and Neumann boundary conditions

for a finite symmetric rectangular domain decomposition were obtained. Further investigations were performed in [25,48], where a detailed analysis on the influence of domain truncations on the performance of optimized Schwarz methods is performed. Circular domain decompositions can be found in [24, 28], see also the scalability study of classical Schwarz methods applied to molecules consisting of chains of circular atoms [10,11], and a new technique based on separation of variables for variable coefficient problems [26]. However, the influence of elliptical geometries on Schwarz methods has been not known so far, and is the second motivation of the present research. Our third motivation is that for Helmholtz problems on elliptical domains, there exists a fast direct solver, which will lead to efficient subdomain solvers if we decompose the elliptically shaped domain into smaller subdomains of elliptical geometry, and can lead to much faster solvers than decomposing the elliptical domain using straight interfaces.

To study OSMs where the interfaces are ellipses, we use elliptic coordinates (ξ, θ), which are linked to the Cartesian coordinates (x, y) for a constant $f > 0$ by the transform

$$\begin{aligned} x &= f \cosh\xi \cos\theta, \;\; 0 \le \xi, \\ y &= f \sinh\xi \sin\theta, \;\; 0 \le \theta < 2\pi. \end{aligned} \tag{2}$$

For any fixed ξ, the corresponding (x, y) describe an ellipse for $0 \le \theta < 2\pi$, with semi-major axis $f \cosh\xi$, semi-minor axis $f \sinh\xi$ and the two foci $(\pm f, 0)$. In these new coordinates (ξ, θ), we consider an elliptical domain for (1) defined for a constant $\bar{\Xi} > 0$ by

$$\Omega := \{(\xi, \theta) | 0 \le \xi < \bar{\Xi}, 0 \le \theta < 2\pi\}. \tag{3}$$

We then define for a second fixed constant Ξ such that $0 < \Xi < \bar{\Xi}$ two subdomains, see Figure 1, as

$$\begin{aligned} \Omega_1 &:= \{(\xi, \theta) | 0 \le \xi < \Xi + L, \; 0 \le \theta < 2\pi\}, \\ \Omega_2 &:= \{(\xi, \theta) | \Xi < \xi < \bar{\Xi}, \; 0 \le \theta < 2\pi\}, \end{aligned} \tag{4}$$

where $L \ge 0$ describes the overlap. The artificial interfaces introduced by this decomposition are $\Gamma_1 := \{(\xi, \theta) | \xi = \Xi + L, \; 0 \le \theta < 2\pi\}$ and $\Gamma_2 := \{(\xi, \theta) | \xi = \Xi, \; 0 \le \theta < 2\pi\}$. A general parallel Schwarz algorithm [16] for this decomposition solves then for iteration index $n = 1, 2, \ldots$ the subdomain problems

$$(\Delta - \eta) u_1^n = g \text{ in } \Omega_1, \quad (\Delta - \eta) u_2^n = g \text{ in } \Omega_2 \tag{5}$$

using for the information exchange between subdomains the transmission conditions

$$\mathcal{B}_1(u_1^n) = \mathcal{B}_1(u_2^{n-1}) \text{ on } \Gamma_1, \quad \mathcal{B}_2(u_2^n) = \mathcal{B}_2(u_1^{n-1}) \quad \text{on } \Gamma_2. \tag{6}$$

Here $\mathcal{B}_1$ and $\mathcal{B}_2$ are transmission operators to be chosen such that the subdomain problems are well posed and the algorithm converges as fast as possible with a low cost for the subdomain solves, comparable to the classical parallel Schwarz method when the transmission operators are the identity. Systematic

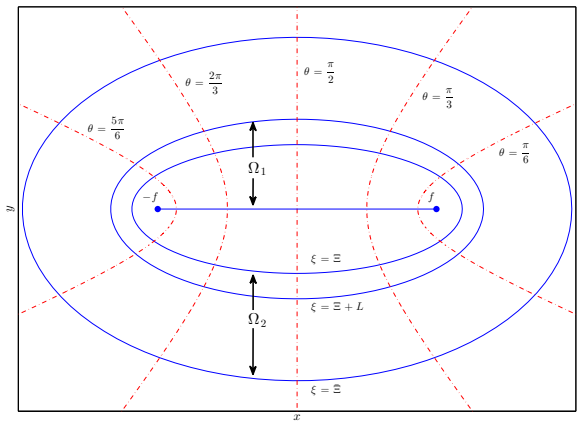

Fig. 1 Illustration of elliptic coordinates and the domain decomposition used in this paper.

methods for determining efficient transmission operators were developed over the last decade for regularly shaped interfaces, see for example [16] for straight lines, [27] for a parabolically shaped interface and [24,28] for circular interfaces. Further analysis shows that the optimized parameters from the straight interface analysis can be properly scaled using the curvature of the circular interface to achieve good performance [28].

The rest of this paper is organized as follows: in Section 2 we analyze the classical Schwarz method and provide a convergence result by introducing the technique of separation of variables and Mathieu like functions. In Section 3 we consider optimized Schwarz methods for both the overlapping and nonoverlapping cases, where a series of transmission conditions, including OO0, OO2 and O2s, are introduced and rigorously optimized for fast convergence using asymptotic analysis. In Section 4, we further discuss unified formulas of optimized transmission parameters highlighted by our analysis when OSMs are applied to different geometric domains, implementation issues and the extension to model problem with variable coefficients. The theoretical results are illustrated using numerical examples in Section 5. We finally draw conclusions in Section 6.

2 The classical Schwarz method

If we choose $\mathcal{B}_i = I$, the identity operator, in the transmission conditions (6), we obtain the classical parallel Schwarz method, which is still widely used, and whose convergence properties we analyze in this section using the technique of separation of variables. In the elliptic coordinates (ξ, θ), the classical Schwarz

method reads

$$\frac{1}{\frac{f^2}{2}(\cosh 2\xi - \cos 2\theta)}\left(\frac{\partial^2 u_i^n}{\partial \xi^2} + \frac{\partial^2 u_i^n}{\partial \theta^2}\right) - \eta u_i^n = g \text{ in } \Omega_i, \text{ for } i = 1,2 \quad (7)$$

with transmission conditions given by

$$u_1^n(\Xi + L, \cdot) = u_2^{n-1}(\Xi + L, \cdot), \quad u_2^n(\Xi, \cdot) = u_1^{n-1}(\Xi, \cdot). \quad (8)$$

By linearity, we only have to analyze the homogeneous case, i.e. $g = 0$, which corresponds to analyzing directly the error equations, see [16].

2.1 Decoupling using separation of variables

The first step of analyzing the classical Schwarz method (5) is typically performing a Fourier transform along the interfaces, which leads to a dimension reduction for a straight/circular interface, and then only ordinary differential equations need to be solved, together with the transmission conditions, to obtain the convergence factor of the method, see [16,24,28] for details. For our elliptical geometry, the Fourier transform is not directly applicable, and we thus use the technique of separation of variables that led originally to the discovery of the Fourier transform by Fourier, and which has been successfully used in [26] for analyzing OSMs with variable reaction term. We thus make the ansatz that the subdomain solutions at each iteration can be written as $u_i^n(\xi, \theta) = R_i(\xi)\Phi(\theta)$, $\Phi(0) = \Phi(2\pi)$ for $i = 1, 2$. Inserting this ansatz into equation (7) with $g = 0$ and dividing each term by $R_i(\xi)\Phi(\theta)$, we obtain after a rearrangement of terms

$$\frac{R_i^{''}}{R_i} - \frac{f^2\eta}{2}\cosh 2\xi = -\frac{\Phi^{''}}{\Phi} - \frac{f^2\eta}{2}\cos 2\theta. \quad (9)$$

Since in (9) the left hand side depends only on ξ and the right hand side depends only on θ, there must exist a constant α such that

$$\frac{R_i^{''}}{R_i} - \frac{f^2\eta}{2}\cosh 2\xi = -\frac{\Phi^{''}}{\Phi} - \frac{f^2\eta}{2}\cos 2\theta = \alpha.$$

Denoting by $\bar{q} := \frac{f^2\eta}{4} > 0$, we thus obtain the two separated equations

$$R_i^{''} - (\alpha + 2\bar{q}\cosh 2\xi)R_i = 0, \quad \xi \in I_i \text{ for } i = 1, 2, \quad (10)$$

with $I_1 = (0, \Xi + l)$, $I_2 = (\Xi, \bar{\Xi})$, and

$$\Phi^{''} + (\alpha + 2\bar{q}\cos 2\theta)\Phi = 0, \ \Phi(0) = \Phi(2\pi). \quad (11)$$

Equation (11) is a Sturm-Liouville eigenvalue problem, where α, which could be negative, is known as the eigenvalue, and $\Phi_\alpha(\theta; \bar{q})$ is the corresponding eigenfunction, which is known as the angular Mathieu function (for a nice

review on Mathieu functions and their computation, see [8]). There exist infinitely many eigenvalues α of (11), and they generate an infinite set of real values which can be ordered, $\alpha_0 < \alpha_1 < \alpha_2 < \ldots$, which we denote by

$$\mathbb{E}: = \{\alpha_0, \alpha_1, \alpha_2, \alpha_3, \ldots\},$$

where α_k is the k-th eigenvalue. For an estimate of the eigenvalue α_k, we have the following lemma (see Section 4 of [46]).

Lemma 1 *For any $\bar{q} > 0$, we have that*

$$k^2 - 2\bar{q} < \alpha_k(\bar{q}) < k^2 + 2\bar{q}, \ k = 1, 2, 3, \ldots \tag{12}$$

Furthermore, the set $\mathbb{E}$ can be separated into the following two disjoint sets:

$$\mathbb{E}_e = \{\alpha_m^e | m = 0, 1, 2, \ldots\}, \quad \mathbb{E}_o = \{\alpha_m^o | m = 1, 2, \ldots\},$$

where $\alpha_m^e = \alpha_{2m-(m \mod 2)}$ for $m = 0, 1, 2, \ldots$ and $\alpha_m^o = \alpha_{2m-((m+1) \mod 2)}$ for $m = 1, 2, \ldots$. In fact, $\mathbb{E}_e$ and $\mathbb{E}_o$ are defined according to the symmetry property of $\Phi_{\alpha_k}(\theta; \bar{q})$: $\Phi_{\alpha_m^e}(\theta; \bar{q})$ are even with respect to $\theta = 0$ and thus are known as even mode angular Mathieu functions, whereas $\Phi_{\alpha_m^o}(\theta; \bar{q})$ are odd with respect to $\theta = 0$ and are known as odd mode angular Mathieu functions. For the properties of angular Mathieu functions, we refer the interested reader to [31]. Because of the nature of the Sturm-Liouville eigenvalue problem (11), we know that the eigenfunctions $\Phi_{\alpha_k}(\theta, \bar{q})$ are uniquely determined up to a constant, and can be properly scaled such that they are orthonormal,

$$\int_0^{2\pi} \Phi_{\alpha_k}(\theta; \bar{q}) \Phi_{\alpha_l}(\theta; \bar{q}) d\theta = \delta_{kl},$$

where δ_{kl} is the Kronecker delta. For more details we refer the reader to [1]. Therefore, the generic subdomain solutions are given by $u_i^n(\xi, \theta) = \sum_{\alpha \in \mathbb{E}} A_{i,\alpha}^n R_{i,\alpha}(\xi; \bar{q}) \Phi_\alpha(\theta; \bar{q})$, the linear combinations of solutions of (10) and (11) corresponding to each eigenmode, where we have shown the dependence on $\bar{q}$, and on α by a subscript α, and in what follows when there is no ambiguity we will omit the dependence on $\bar{q}$ for simplicity. Inserting these generic subdomain solutions into the transmission conditions (8) we obtain

$$\begin{array}{c} \sum_{\alpha \in \mathbb{E}} A_{1,\alpha}^n R_{1,\alpha}(\Xi + L) \Phi_\alpha(\theta) = \sum_{\alpha \in \mathbb{E}} A_{2,\alpha}^{n-1} R_{2,\alpha}(\Xi + L) \Phi_\alpha(\theta), \\ \sum_{\alpha \in \mathbb{E}} A_{2,\alpha}^n R_{2,\alpha}(\Xi) \Phi_\alpha(\theta) = \sum_{\alpha \in \mathbb{E}} A_{1,\alpha}^{n-1} R_{1,\alpha}(\Xi) \Phi_\alpha(\theta). \end{array} \tag{13}$$

Now, choosing a $\beta \in \mathbb{E}$ different from α, multiplying by $\Phi_\beta(\theta)$ on both sides of the equations in (13) and integrating from 0 to 2π, we obtain using orthonormality

$$A_{1,\alpha}^n R_{1,\alpha}(\Xi + L) = A_{2,\alpha}^{n-1} R_{2,\alpha}^{n-1}(\Xi + L), \quad A_{2,\alpha}^n R_{2,\alpha}(\Xi) = A_{1,\alpha}^{n-1} R_{1,\alpha}(\Xi).$$

The classical Schwarz method thus corresponds to solving at iteration n for each α the ordinary differential equations

$$R_{1,\alpha}'' - (\alpha + 2\bar{q} \cosh 2\xi) R_{1,\alpha} = 0, \ R_{1,\alpha}(\Xi + L) = \frac{A_{2,\alpha}^{n-1}}{A_{1,\alpha}^n} R_{2,\alpha}(\Xi + L), \tag{14}$$

and

$$R_{2,\alpha}^{''}-(\alpha+2\bar{q}\cosh 2\xi)R_{2,\alpha}=0,\ R_{2,\alpha}(\Xi)=\frac{A_{1,\alpha}^{n-1}}{A_{2,\alpha}^{n}}R_{1,\alpha}(\Xi),\ R_{2,\alpha}(\bar{\Xi})=0. \quad (15)$$

The subproblem (15) is now a well-defined two-point boundary value problem on the interval $(\Xi,\bar{\Xi})$. The problem (14) is however not mathematically closed, one needs to add a boundary condition at $\xi=0$, which can be obtained by analyzing the symmetry property of the undecoupled original problem as follows: for every $\alpha\in\mathbb{E}_e$, the function $\Phi_\alpha(\theta)$ is even in θ, and thus $R_{1,\alpha}(\xi)\Phi_\alpha(\theta)=R_{1,\alpha}(\xi)\Phi_\alpha(-\theta)$ for $\theta\in(0,\pi)$ and $\xi\in(0,\Xi+L)$, which implies that we must have $\frac{d}{d\xi}R_{1,\alpha}(0)=0$. For every $\alpha\in\mathbb{E}_o$, the function $\Phi_\alpha(\theta)$ is odd in θ, and thus $R_{1,\alpha}(\xi)\Phi_\alpha(\theta)=-R_{1,\alpha}(\xi)\Phi_\alpha(-\theta)$ for $\theta\in(0,\pi)$ and $\xi\in(0,\Xi+L)$, which implies that $R_{1,\alpha}(0)=0$. Hence the additional boundary condition for problem (14) is

$$R_{1,\alpha}^{'}(0)=0 \text{ for } \alpha\in\mathbb{E}_e, \quad \text{and} \quad R_{1,\alpha}(0)=0 \text{ for } \alpha\in\mathbb{E}_o. \quad (16)$$

2.2 Properties of the radial Mathieu like functions

The differential equation in (10) is known as the radial Mathieu equation, and its solutions are called the radial Mathieu functions when defined for all $\xi>0$. In our case however, the subproblems (14,16) and (15) consist of the differential equation in (10) posed on a finite interval with suitable boundary conditions. We therefore call the corresponding solutions the radial Mathieu like functions. In particular, we denote by $M\!I_\alpha(\xi)$ the solutions to problem (14,16), and by $M\!K_\alpha(\xi)$ the solutions to problem (15), according to their monotonicities and the similarity with the modified Bessel functions as we show below.

We thus now investigate for $\alpha\in\mathbb{E}$ the solution properties of the two-point boundary value problems

$$\begin{aligned}(M\!I_\alpha)^{''}-(\alpha+2\bar{q}\cosh 2\xi)M\!I_\alpha=0,\quad \xi\in(0,a)\\ M\!I_\alpha(a)=\omega,\\ M\!I_\alpha^{'}(0)=0 \text{ for } \alpha\in\mathbb{E}_e,\\ M\!I_\alpha(0)=0 \text{ for } \alpha\in\mathbb{E}_o,\end{aligned} \quad (17)$$

where a and ω are positive constants, and

$$(M\!K_\alpha)^{''}-(\alpha+2\bar{q}\cosh 2\xi)M\!K_\alpha=0,\quad M\!K_\alpha(a)=\omega,\quad M\!K_\alpha(b)=0, \quad (18)$$

where $b>a>0$ and $\omega>0$ are constants.

Lemma 2 *For any given $\alpha\in\mathbb{E}$, the function $M\!I_\alpha(\xi)$ is monotonically increasing in ξ, and the function $M\!K_\alpha(\xi)$ is monotonically decreasing in ξ.*

Proof For any given $\alpha \in \mathbb{E}$, applying the maximum principle shows that the function $M\!I_\alpha(\xi)$ reaches its maximum or its minimum on the boundary. Since $M\!K_\alpha(a) > M\!K_\alpha(b) = 0$, we must therefore have that $M\!K_\alpha(\xi)$ is monotonically decreasing in ξ for $\xi \in (a, b)$. A similar argument also applies for $M\!I_\alpha(\xi)$ if $\alpha \in \mathbb{E}_o$ and shows that $M\!I_\alpha(\xi)$ is monotonically increasing in ξ for $\xi \in (0, a)$. If $\alpha \in \mathbb{E}_e$, we also claim that we must have $M\!I_\alpha(0) < M\!I_\alpha(a)$. This is because $M\!I_\alpha(0) \geq M\!I_\alpha(a)$ leads to a contradiction as follows: if $M\!I_\alpha(0) = M\!I_\alpha(a) = \omega$, by the maximum principle, we obtain $M\!I_\alpha(\xi) = \omega$ a constant for $\xi \in (0, a)$. However, a nonzero constant function does not satisfy the defining equation in (17), and we have a contradiction. If $M\!I_\alpha(0) > M\!I_\alpha(a)$, we must have by the maximum principle that the function $M\!I_\alpha(\xi)$ is monotonically decreasing in ξ for $\xi \in (0, a)$, and it must in particular be positive. Thus, $M\!I_\alpha^{''}(\xi) = (\alpha + 2\bar{q}\cosh 2\xi) M\!I_\alpha(\xi) > 0$ for $\xi \in (0, a)$ because both factors on the right are positive. Now, for any positive $\epsilon \in (0, a)$ we integrate this differential equation on $(0, \epsilon)$ to obtain

$$M\!I_\alpha^{'}(\epsilon) = \int_0^\epsilon (\alpha + 2\bar{q}\cosh 2\xi) M\!I_\alpha(\xi) d\xi + M\!I_\alpha^{'}(0) > 0,$$

since $M\!I_\alpha^{'}(0) = 0$ and the integrand is positive. Thus, the function $M\!I_\alpha(\xi)$ is monotonically increasing instead of decreasing, again a contradiction. Therefore $M\!I_\alpha(0) < M\!I_\alpha(a) = \omega$, which, again, by the maximum principle shows that $M\!I_\alpha(\xi)$ increases monotonically in ξ for $\xi \in (0, a)$. □

Lemma 3 *For any given $\alpha \in \mathbb{E}$, the functions $M\!I_\alpha(\xi)$ ($\xi \in (0, a)$) and $M\!K_\alpha(\xi)$ ($\xi \in (a, b)$) are positive.*

Proof Clearly, $M\!K_\alpha(\xi)$ is positive because of the positive boundary condition at $\xi = a$ and the monotonicity property proved in Lemma 2, and a similar argument applies for $M\!I_\alpha(\xi)$ when $\alpha \in \mathbb{E}_o$, since then a homogeneous Dirichlet boundary condition is applied at $\xi = 0$. We then only need to show the positiveness for $M\!I_\alpha(\xi)$ when $\alpha \in \mathbb{E}_e$, which we show again by contradiction. We thus assume that the function $M\!I_{\alpha_m^e}(\xi)$ is not always positive. Because of the monotonicity property proved in Lemma 2, we must have $M\!I_{\alpha_m^e}(0) < 0$, which, together with the boundary condition $M\!I_{\alpha_m^e}^{'}(0) = 0$ and the above-mentioned monotonicity property, shows that $M\!I_{\alpha_m^e}^{''}(0) > 0$. However, from the equation we have $M\!I_{\alpha_m^e}^{''}(0) = (\alpha_m^e + 2\bar{q}\cosh 2\xi) M\!I_{\alpha_m^e}(0) < 0$ since $\alpha_m^e + 2\bar{q}\cosh 2\xi$ is positive, which is a contradiction. □

We proved the results in Lemma 3 using Lemma 2. We now show in turn that the results in Lemma 3 can be used to further sharpen the results of of Lemma 2.

Lemma 4 *For any given $\alpha \in \mathbb{E}$, the function $M\!I_\alpha(\xi)$ is strictly monotonically increasing in ξ for $\xi \in (0, a)$, and the function $M\!K_\alpha(\xi)$ is strictly monotonically decreasing in ξ for $\xi \in (a, b)$.*

Proof We only prove the result for $MI_\alpha(\xi)$, the result for $MK_\alpha(\xi)$ can be proved similarly. Using Lemma 3, we obtain for any $\xi_1, \xi_2 \in (0,a)$ satisfying $\xi_2 > \xi_1$ that

$$\int_{\xi_1}^{\xi_2} MI_\alpha^{''}(\xi)d\xi = \int_{\xi_1}^{\xi_2} (\alpha + 2\bar{q}\cosh 2\xi) MI_\alpha(\xi)d\xi > 0,$$

which shows that $MI_\alpha^{'}(\xi_2) > MI_\alpha^{'}(\xi_1)$. Together with Lemma 2, this concludes the proof. □

Lemma 5 *The following assertions hold:*

a) The function $MK_\alpha(\xi)$ is strictly monotonically decreasing in α for any fixed $\xi \in (a,b)$.
b) For any fixed $\xi \in (0,a)$, the function $MI_\alpha(\xi)$ is strictly monotonically decreasing in α for $\alpha \in \mathbb{E}_e$ or $\alpha \in \mathbb{E}_o$.
c) For $\xi \in (0,a)$ it holds that $MI_{\alpha_0^e}(\xi) > MI_\alpha(\xi)$ for all $\alpha \in \mathbb{E}\backslash\{\alpha_0^e\}$; for $\xi \in (a,b)$ it holds that $MK_{\alpha_0^e}(\xi) > MK_\alpha(\xi)$ for all $\alpha \in \mathbb{E}\backslash\{\alpha_0^e\}$.

Proof a) Assume that α_1 and α_2 are the eigenvalues of the Sturm-Liouville problem (11) satisfying $\alpha_2 > \alpha_1$; we then have

$$MK_{\alpha_1}^{''} - (\alpha_1 + 2\bar{q}\cosh 2\xi) MK_{\alpha_1} = 0, \tag{19}$$

and

$$MK_{\alpha_2}^{''} - (\alpha_2 + 2\bar{q}\cosh 2\xi) MK_{\alpha_2} = 0. \tag{20}$$

Subtracting (19) from (20) we obtain

$$(MK_{\alpha_2} - MK_{\alpha_1})^{''} - (\alpha_1 + 2\bar{q}\cosh 2\xi)(MK_{\alpha_2} - MK_{\alpha_1}) = (\alpha_2 - \alpha_1) MK_{\alpha_2} > 0, \tag{21}$$

since $MK_\alpha > 0$ for any $\alpha \in \mathbb{E}$ as shown previously. Hence, applying the maximum principle to the equation (21) shows that $MK_{\alpha_2} - MK_{\alpha_1}$ is non-positive for all $\xi \in (a,b)$. If $MK_{\alpha_2}(\xi) = MK_{\alpha_1}(\xi)$ for all $\xi \in (a,b)$, then equation (21) reads $0 = (\alpha_2 - \alpha_1) MK_{\alpha_2} > 0$, which is a contradiction. If at some $\bar{\xi} \in (a,b)$ we had $MK_{\alpha_2}(\bar{\xi}) = MK_{\alpha_1}(\bar{\xi})$, then there exists a small $\epsilon > 0$ such that $(MK_{\alpha_2} - MK_{\alpha_1})^{'}(\xi) > 0$ in $(\bar{\xi} - \epsilon, \bar{\xi})$ and $(MK_{\alpha_2} - MK_{\alpha_1})^{'}(\xi) < 0$ in $(\bar{\xi}, \bar{\xi} + \epsilon)$; we thus would have $(MK_{\alpha_2} - MK_{\alpha_1})^{''}(\bar{\xi}) < 0$, which is a contradiction to equation (21). Therefore $(MK_{\alpha_2} - MK_{\alpha_1})(\xi) < 0$ must hold for all $\xi \in (a,b)$.

b) For $\alpha \in \mathbb{E}_o$, the proof is similar to the proof of a). When $\alpha \in \mathbb{E}_e$, from the proof of a), we only need to show that $MI_{\alpha_2}(0) < MI_{\alpha_1}(0)$ for the even mode eigenvalues $\alpha_2 > \alpha_1$, which we do now again by contradiction. We thus assume that $MI_{\alpha_2}(0) \geq MI_{\alpha_1}(0)$. When equality holds, from the proof of a), we know that $MI_{\alpha_1}(\xi) < MI_{\alpha_2}(\xi)$ for $\xi \in (0,a)$, which contradicts the fact that $MI_{\alpha_2}^{'}(0) = MI_{\alpha_1}^{'}(0)$ and both $MI_{\alpha_2}(\xi)$ and $MI_{\alpha_1}(\xi)$ are convex in $(0,a)$. When the strict inequality holds, i.e. $MI_{\alpha_2}(0) > MI_{\alpha_1}(0)$, we assume that $MI_{\alpha_2}(\xi) > MI_{\alpha_1}(\xi)$ in $(0,a)$, since otherwise we would simply need

to consider the smaller interval $(0, \bar{\xi})$, where $\bar{\xi}$ is the point where the two function values $M\!I_{\alpha_2}(\bar{\xi})$ and $M\!I_{\alpha_1}(\bar{\xi})$ are equal. Now we have by Lemma 3

$$(M\!I_{\alpha_2} - M\!I_{\alpha_1})'' = (\alpha_1 + 2\bar{q}\cosh 2\xi)(M\!I_{\alpha_2} - M\!I_{\alpha_1}) + (\alpha_2 - \alpha_1)M\!I_{\alpha_1} > 0.$$

Integrating this equation from zero to ϵ, where $\epsilon \in (0, a)$, we arrive at

$$\int_0^{\epsilon} (M\!I_{\alpha_2} - M\!I_{\alpha_1})'' d\xi > 0,$$

which gives

$$M\!I'_{\alpha_2}(\epsilon) - M\!I'_{\alpha_1}(\epsilon) > 0.$$

Since this relation holds for each ϵ, we can integrate it from zero to a to obtain

$$M\!I_{\alpha_2}(a) - M\!I_{\alpha_2}(0) > M\!I_{\alpha_1}(a) - M\!I_{\alpha_1}(0)$$

which means by noting that $M\!I_{\alpha_1}(a) = M\!I_{\alpha_2}(a)$ that we have $M\!I_{\alpha_2}(0) < M\!I_{\alpha_1}(0)$, which is a contradiction.

c) For any $\alpha \in \mathbb{E}\backslash\{\alpha_0^e\}$, we denote by $D(\xi)$: $= M\!I_{\alpha_0^e}(\xi) - M\!I_{\alpha}(\xi)$. Then, the function $D(\xi)$ satisfies the equation

$$D''(\xi) - (\alpha_e^0 + 2\bar{q}\cosh 2\xi)D(\xi) = (\alpha_e^0 - \alpha)M\!I_{\alpha}(\xi) < 0.$$

Noting that $D(a) = 0$ and $D(0) > 0$, we then have by the maximum principle that $D(\xi) \geq 0$ for $\xi \in (0, a)$. In fact, a strict inequality holds, i.e., $D(\xi) > 0$ for $\xi \in (0, a)$. Otherwise, by a similar argument as in the proof of b) we reach a contradiction. The remaining part can then be proved in a similar fashion.

□

Denoting by $w_\alpha(\xi)$: $= \frac{M\!I'_\alpha(\xi)}{M\!I_\alpha(\xi)}$ and $v_\alpha(\xi)$: $= \frac{M\!K'_\alpha(\xi)}{M\!K_\alpha(\xi)}$, we obtain the following lemma on the monotonicity of w_α and v_α as a function of α.

Lemma 6 *For $\xi \in (0, a)$, $w_\alpha(\xi)$ is positive and increases monotonically in α for $\alpha \in \mathbb{E}_e$ and $\alpha \in \mathbb{E}_o$. In particular, we have that $w_{\alpha_0^e}(\xi) < w_{\alpha_1^o}(\xi)$. For $\xi \in [a, b)$, $v_\alpha(\xi)$ is negative and decreases monotonically in α for $\alpha \in \mathbb{E}$.*

Proof The positivity of w_α and $-v_\alpha$ can be obtained directly from the monotonicity of $M\!I_\alpha(\xi)$ and $M\!K_\alpha(\xi)$ shown in Lemma 5. By the Chaplygin type comparison theorem for nonlinear ordinary differential equations [9], we then need only to show the results at the end point a. Using the second assertion in Lemma 5 we find that $M\!I_{\alpha_1}(\xi) > M\!I_{\alpha_2}(\xi)$ for any $\alpha_2 > \alpha_1 \in \mathbb{E}_e$; thus we have $w_{\alpha_1}(a) < w_{\alpha_2}(a)$, where we have used the fact that $M\!I_{\alpha_1}(a) = M\!I_{\alpha_2}(a)$ and the convexity of $M\!I_\alpha(\xi)$ for any $\alpha \in \mathbb{E}_e$. For $\alpha \in \mathbb{E}_o$, the proof is similar. An application of the third assertion in Lemma 5 then shows that $w_{\alpha_0^e}(a) < w_{\alpha_1^o}(a)$. The second part of this lemma can be shown in a similar fashion. □

2.3 Convergence analysis

We now return to the analysis of the classical Schwarz method (7,8). From the separation of variables ansatz, we find that the subdomain solutions of (7) are of the form

$$u_1^n(\xi,\theta) = \sum_{\alpha\in\mathbb{E}_e} A_{1,\alpha^e}^n \mathit{MI}_{\alpha^e}(\xi)\Phi_{\alpha^e}(\theta) + \sum_{\alpha\in\mathbb{E}_o} A_{1,\alpha^o}^n \mathit{MI}_{\alpha^o}(\xi)\Phi_{\alpha^o}(\theta),$$

and

$$u_2^n(\xi,\theta) = \sum_{\alpha\in\mathbb{E}_e} A_{2,\alpha^e}^n \mathit{MK}_{\alpha^e}(\xi)\Phi_{\alpha^e}(\theta) + \sum_{\alpha\in\mathbb{E}_o} A_{2,\alpha^o}^n \mathit{MK}_{\alpha^o}(\xi)\Phi_{\alpha^o}(\theta).$$

Inserting this into the transmission conditions (8) and using the orthonormal property of angular Mathieu functions we obtain

$$A_{1,\alpha}^n \mathit{MI}_\alpha(\Xi+L) = A_{2,\alpha}^{n-1}\mathit{MK}_\alpha(\Xi+L),\ A_{2,\alpha}^n \mathit{MK}_\alpha^n(\Xi) = A_{1,\alpha}^{n-1}\mathit{MI}_\alpha^{n-1}(\Xi),\ \alpha\in\mathbb{E}. \tag{22}$$

By iterating between subdomains Ω_1 and Ω_2, we obtain for each $\alpha\in\mathbb{E}$

$$A_{1,\alpha}^{2n} = \rho_{cla}^n A_{1,\alpha}^0, \quad A_{2,\alpha}^{2n} = \rho_{cla}^n A_{2,\alpha}^0, \tag{23}$$

with the convergence factor ρ_{cla} given by

$$\rho_{cla}(\alpha,\Xi,L) := \frac{\mathit{MK}_\alpha(\Xi+L)}{\mathit{MI}_\alpha(\Xi+L)}\cdot\frac{\mathit{MI}_\alpha(\Xi)}{\mathit{MK}_\alpha(\Xi)}. \tag{24}$$

Theorem 1 *The classical Schwarz method (7,8) converges if and only if there is overlap, $L>0$, and for L small, we have the convergence factor estimate*

$$\max_{\alpha\in\mathbb{E}}\rho_{cla} = 1 - G_{\min}L + O(L^2),$$

where $G_{\min} = \min_{\alpha\in\mathbb{E}} G(\alpha,\Xi) = G(\alpha_0^e,\Xi)$ with $G(\alpha,\xi)$ defined by $G(\alpha,\xi) := \frac{\mathit{MI}_\alpha'(\xi)}{\mathit{MI}_\alpha(\xi)} - \frac{\mathit{MK}_\alpha'(\xi)}{\mathit{MK}_\alpha(\xi)} = w_\alpha(\xi) - v_\alpha(\xi)$, where the prime denotes the derivative in ξ.

Proof Since for $\bar{q}>0$ and any $\alpha\in\mathbb{E}$, the Mathieu like function $\mathit{MI}_\alpha(\xi)$ is positive and increasing in ξ, and $\mathit{MK}_\alpha(\xi)$ is positive and decreasing in ξ, we have that $0<\rho_{cla}<1$ if and only if the overlap $L>0$. A Taylor expansion of the convergence factor $\rho_{cla}(\alpha,\Xi,L)$ in L at zero then gives

$$\rho_{cla} = 1 - G(\alpha,\Xi)L + O(L^2).$$

Using Lemma 6, we find that the function $G(\alpha,\xi)$ attains its minimum at $\alpha=\alpha_0^e$, and hence the convergence factor ρ_{cla} attains its maximum at $\alpha=\alpha_0^e$ asymptotically, which concludes the proof. □

Remark 1 Comparing Theorem 1 with Theorem 2.3 in [24], we find that our new result becomes the one for the circular domain decomposition when we replace $G_{\min}$ in Theorem 1 by the constant $\sqrt{\eta}G_{\min}$ in [24]. We will see that this also holds for the optimized transmission conditions we study next.

3 Optimized transmission conditions

For faster convergence, we choose the transmission operators as $\mathcal{B}_i = \partial_\xi + \mathcal{S}_i$ $(i = 1, 2)$, with $\mathcal{S}_i$ linear operators along the interface Γ_i to be determined such that the corresponding Schwarz methods are well defined and converge as fast as possible with cost per iteration comparable to the classical Schwarz method. The transmission conditions then are

$$\begin{aligned} (\partial_\xi + \mathcal{S}_1)u_1^n &= (\partial_\xi + \mathcal{S}_1)u_2^{n-1} \text{ on } \Gamma_1, \\ (\partial_\xi + \mathcal{S}_2)u_2^n &= (\partial_\xi + \mathcal{S}_2)u_1^{n-1} \text{ on } \Gamma_2. \end{aligned} \tag{25}$$

Together with the subdomain problems (7), this defines an optimized parallel Schwarz methods for elliptical domain decompositions. To determine the best transmission operators $\mathcal{S}_i$, it suffices again to only study the error equations when $g = 0$.

Similar to the analysis for the classical Schwarz method, inserting the generic subdomain solutions $u_i^n(\xi, \theta) = \sum_{\alpha\in\mathbb{E}} A_{i,\alpha}^n R_{i,\alpha}(\xi)\Phi_\alpha(\theta)$ into (7), we obtain by the orthonormality of $\Phi_\alpha(\theta)$ for each $\alpha \in \mathbb{E}$

$$R_{i,\alpha}^{''} - (\alpha + 2\bar{q}\cosh 2\xi)R_{i,\alpha} = 0, \quad \xi \in I_i, \ i = 1, 2, \tag{26}$$

where again we use a subscript α to indicate the dependence on α. Inserting $u_i^n(\xi, \theta) = \sum_{\alpha\in\mathbb{E}} A_{i,\alpha}^n R_{i,\alpha}(\xi)\Phi_\alpha(\theta)$ also into the transmission conditions (25) and using orthonormality again, we find

$$\begin{aligned} A_{1,\alpha}^n(R_{1,\alpha}^{'} + \sigma_1(\alpha)R_{1,\alpha}) &= A_{2,\alpha}^{n-1}(R_{2,\alpha}^{'} + \sigma_1(\alpha)R_{2,\alpha}) \text{ at } \xi = \Xi + L, \\ A_{2,\alpha}^n(R_{2,\alpha}^{'} + \sigma_2(\alpha)R_{2,\alpha}) &= A_{1,\alpha}^{n-1}(R_{1,\alpha}^{'} + \sigma_2(\alpha)R_{1,\alpha}) \text{ at } \xi = \Xi, \end{aligned} \tag{27}$$

where $\alpha \in \mathbb{E}$ and the $\sigma_i(\alpha)$ are the symbols of the operators $\mathcal{S}_i$, $i = 1, 2$ associated with the eigenfunctions $\Phi_\alpha(\theta)$ defined for any smooth function $h(\theta)$ in $(0, 2\pi)$ by

$$\int_0^{2\pi} (\mathcal{S}_i h(\theta))\Phi_\alpha(\theta)d\theta = \sigma_i(\alpha) \int_0^{2\pi} h(\theta)\Phi_\alpha(\theta)d\theta.$$

Thus, the first separated subdomain problem should satisfy boundary conditions at zero as described in subsection 2.1 and at $\Xi + L$ a Robin boundary condition. The second separated subdomain problem should satisfy a homogeneous Dirichlet boundary condition at $\xi = \bar{\Xi}$ and at Ξ again a Robin boundary condition. Then, by a Robin-to-Dirichlet operator, these Robin transmission conditions are equivalent to some Dirichlet boundary conditions, and we find that the subdomain solutions of (26) are given respectively by $M\mathit{I}_\alpha(\xi)$ and $M\mathit{K}_\alpha(\xi)$. Inserting these solutions into (27), we obtain by induction

$$A_{1,\alpha}^{2n} = \rho_{opt}^n A_{1,\alpha}^0, \quad A_{2,\alpha}^{2n} = \rho_{opt}^n A_{2,\alpha}^0, \tag{28}$$

where the convergence factor ρ_{opt} is given by

$$\begin{aligned} &\rho_{opt}(\alpha, \Xi, L, \sigma_1(\alpha), \sigma_2(\alpha)) \\ &\quad = \frac{-v_\alpha(\Xi + L) + \sigma_1(\alpha)}{w_\alpha(\Xi + L) + \sigma_1(\alpha)} \cdot \frac{w_\alpha(\Xi) + \sigma_2(\alpha)}{-v_\alpha(\Xi) + \sigma_2(\alpha)} \cdot \rho_{cla}(\alpha, \Xi, L). \end{aligned} \tag{29}$$

We see that choosing $\sigma_1(\alpha) := v_\alpha(\Xi + L)$ and $\sigma_2(\alpha) := -w_\alpha(\Xi)$ would lead to convergence in two-steps, since then the convergence factor vanishes identically. This leads to a so called optimal Schwarz method, a direct solver, which requires however non-local transmission conditions needing a convolution operation when the symbols are backtransformed. Subdomain iterations are then substantially more expensive than the ones in the classical Schwarz method [16], but many new such algorithms emerged over the last decade, see [30] for an overview.

In this paper, we propose to look for local approximations of $\sigma_i(\alpha)$ of the form

$$\sigma_1^{app}(\alpha) = p_1 + q_1\alpha, \quad \sigma_2^{app}(\alpha) = -p_2 - q_2\alpha, \tag{30}$$

with constants $p_i > 0$, $q_i \geq 0$. The corresponding transmission operators $\mathcal{S}_i$ are

$$\mathcal{S}_1^{app} = p_1 - q_1\partial_{\theta\theta} - 2\bar{q}q_1\cos 2\theta, \quad \mathcal{S}_2^{app} = -p_2 + q_2\partial_{\theta\theta} + 2\bar{q}q_2\cos 2\theta.$$

Replacing $\sigma_i(\alpha)$ by $\sigma_i^{app}(\alpha)$ in the convergence factor ρ_{opt}, we arrive at the convergence factor with local transmission conditions

$$\begin{aligned}&\rho(\alpha, \Xi, L, p_1, p_2, q_1, q_2)\\ &\quad = \frac{v_\alpha(\Xi + L) - p_1 - q_1\alpha}{w_\alpha(\Xi + L) + p_1 + q_1\alpha} \cdot \frac{w_\alpha(\Xi) - p_2 - q_2\alpha}{v_\alpha(\Xi) + p_2 + q_2\alpha} \cdot \rho_{cla}(\alpha, \Xi, L).\end{aligned} \tag{31}$$

To obtain the fastest possible algorithm, the free parameters $p_i, q_i, i = 1, 2$ should then be determined by the min-max problem

$$\min_{p_i>0, q_i\geq 0} \max_{\alpha\in\tilde{\mathbb{E}}} |\rho(\alpha, \Xi, L, p_1, p_2, q_1, q_2)|. \tag{32}$$

For the overlapping case $L > 0$, the set $\tilde{\mathbb{E}}$ can be chosen directly as $\mathbb{E}$, the eigenvalues of the Sturm-Liouville problem (11); for the nonoverlapping case, we need according to [16] a finite truncation of the eigenvalue set $\mathbb{E}$ of the Sturm-Liouville problem (11),

$$\mathbb{E}_N = \{\alpha_{\min} = \alpha_0, \alpha_1, \ldots, \alpha_{\max} = \alpha_N\}$$

and choose $\tilde{\mathbb{E}} = \mathbb{E}_N$, where N is the number of mesh points along the interface when a uniform mesh in the θ-direction is used.

However, it is not easy to solve the optimization problem (32) directly, because of the Mathieu like functions and their derivatives in the convergence factor. We therefore use the technique applied in [24,28] to asymptotically solve the min-max problem (32). To this end, we introduce the following approximation of the convergence factor ρ:

$$\begin{aligned}&\rho_{app}(\alpha, \Xi, L, p_1, p_2, q_1, q_2) :=\\ &\quad \tfrac{\sqrt{\alpha+2\bar{q}\cosh 2\Xi} - p_1 - q_1\alpha}{\sqrt{\alpha+2\bar{q}\cosh 2\Xi} + p_1 + q_1\alpha} \cdot \tfrac{\sqrt{\alpha+2\bar{q}\cosh 2\Xi} - p_2 - q_2\alpha}{\sqrt{\alpha+2\bar{q}\cosh 2\Xi} + p_2 + q_2\alpha} \cdot e^{-2\sqrt{\alpha+2\bar{q}\cosh 2\Xi}L}.\end{aligned} \tag{33}$$

Lemma 7 *For $L \geq 0$ small and α large, both functions $w_\alpha(\Xi+L)$ and $v_\alpha(\Xi+L)$ behave like*

$$\begin{aligned}
&- v_\alpha(\Xi + L) \sim w_\alpha(\Xi + L) \\
&\sim \sqrt{\alpha + 2\bar{q}\cosh 2(\Xi + L)} + O\left((\alpha + 2\bar{q}\cosh 2(\Xi + L))^{-\frac{1}{2}}\right) \\
&= \sqrt{\alpha + 2\bar{q}\cosh 2\Xi} + \frac{\bar{q}\sinh 2\Xi_L}{\sqrt{\alpha + 2\bar{q}\cosh 2\Xi_L}} L + O\left((\alpha + 2\bar{q}\cosh 2(\Xi + L))^{-\frac{1}{2}}\right),
\end{aligned}$$

where Ξ_L lies in between Ξ and $\Xi + L$.

Proof We prove only the result for w_α, the result for $-v_\alpha$ can be obtained similarly. We know that w_α satisfies the equation

$$w_\alpha^{'} + w_\alpha^2 - (\alpha + 2\bar{q}\cosh 2\xi) = 0. \tag{34}$$

For any given $\xi_0 > 0$, we rewrite this equation as

$$w_\alpha^{'} + w_\alpha^2 - (\alpha + 2\bar{q}\cosh 2\xi_0) + 2\bar{q}(\cosh 2\xi_0 - \cosh 2\xi) = 0. \tag{35}$$

Let $\epsilon := (\alpha + 2\bar{q}\cosh 2\xi_0)^{-1}$. Then ϵ goes to zero when α goes to infinity. We then make the ansatz that the solution w_α has the expansion $w_\alpha = \frac{1}{\sqrt{\epsilon}} w_0 + w_1 + \sqrt{\epsilon} w_2 + \epsilon w_3 + \ldots$, where $w_0, w_1, w_2, w_3, \ldots$ are functions of ξ but independent of ϵ. Inserting this ansatz into equation (35), and setting the coefficients of each term in ϵ to zero, we obtain

$$\begin{aligned}
w_0^2 - 1 &= 0, \\
w_0^{'} + 2w_0 w_1 &= 0, \\
w_1^{'} + 2w_0 w_2 + w_1^2 + 2\bar{q}(\cosh 2\xi_0 - \cosh 2\xi) &= 0, \\
w_2^{'} + 2w_0 w_3 + 2w_1 w_2 &= 0, \\
&\cdots
\end{aligned} \tag{36}$$

Solving these equations gives $w_0 = 1$, $w_1 = 0$, $w_2 = \bar{q}(\cosh 2\xi - \cosh 2\xi_0)$, $w_3 = -\sinh 2\xi$, and thus $w_\alpha(\xi_0) = \sqrt{\alpha + 2\bar{q}\cosh 2\xi_0} + O\left((\alpha + 2\bar{q}\cosh 2\xi_0)^{-1}\right)$.

Choosing $\xi_0 = \Xi + L$ and using a Taylor expansion in L for L small gives then the second result.

□

Theorem 2 (Approximation of the convergence factor) *The difference between the convergence factor ρ and its approximation ρ_{app} satisfies the asymptotic estimate*

$$|\rho - \rho_{app}| = \begin{cases} O\left(L^{\min(1-\frac{\gamma}{2}, \frac{3}{2}\gamma)}\right), & L \to 0^+, \alpha = O(L^{-\gamma}), 0 < \gamma < 1, \\ O\left((\alpha + 2\bar{q}\cosh 2\Xi)^{-\frac{3}{2}}\right), & L = 0, \alpha \to \infty. \end{cases} \tag{37}$$

Proof We introduce the abbreviations

$$\rho_1 := \frac{v_\alpha(\Xi+L)-p_1-q_1\alpha}{w_\alpha(\Xi+L)+p_1+q_1\alpha}, \qquad \rho_1^{app} := \frac{\sqrt{\alpha+2\bar{q}\cosh 2\Xi}-p_1-q_1\alpha}{\sqrt{\alpha+2\bar{q}\cosh 2\Xi}+p_1+q_1\alpha},$$
$$\rho_2 := \frac{w_\alpha(\Xi)-p_2-q_2\alpha}{v_\alpha(\Xi)+p_2+q_2\alpha}, \qquad \rho_2^{app} := \frac{\sqrt{\alpha+2\bar{q}\cosh 2\Xi}-p_2-q_2\alpha}{\sqrt{\alpha+2\bar{q}\cosh 2\Xi}+p_2+q_2\alpha},$$
$$\rho_{cla}^{app} := e^{-2\sqrt{\alpha+2\bar{q}\cosh 2\Xi}L}.$$

We then can write the convergence factors in compact form,

$$\rho = \rho_1 \cdot \rho_2 \cdot \rho_{cla}, \quad \rho_{app} = \rho_1^{app} \cdot \rho_2^{app} \cdot \rho_{cla}^{app},$$

which shows that the estimate (37) can be analyzed one by one.

Now we estimate

$$\begin{aligned}
|\rho_1 - \rho_1^{app}| &= \left| \tfrac{v_\alpha(\Xi+L)-p_1-q_1\alpha}{w_\alpha(\Xi+L)+p_1+q_1\alpha} - \tfrac{\sqrt{\alpha+2\bar{q}\cosh 2\Xi}-p_1-q_1\alpha}{\sqrt{\alpha+2\bar{q}\cosh 2\Xi}+p_1+q_1\alpha} \right| \\
&= \left| \tfrac{\sqrt{\alpha+2\bar{q}\cosh 2\Xi}-p_1-q_1\alpha+\varepsilon}{\sqrt{\alpha+2\bar{q}\cosh 2\Xi}+p_1+q_1\alpha+\varepsilon} - \tfrac{\sqrt{\alpha+2\bar{q}\cosh 2\Xi}-p_1-q_1\alpha}{\sqrt{\alpha+2\bar{q}\cosh 2\Xi}+p_1+q_1\alpha} \right| \\
&= \frac{2(p_1+q_1\alpha)\varepsilon}{(\sqrt{\alpha+2\bar{q}\cosh 2\Xi}+p_1+q_1\alpha)(\sqrt{\alpha+2\bar{q}\cosh 2\Xi}+p_1+q_1\alpha+\varepsilon)} \\
&< \frac{2\varepsilon}{\sqrt{\alpha+2\bar{q}\cosh 2\Xi}+p_1+q_1\alpha} \\
&< \frac{2\varepsilon}{\sqrt{\alpha+2\bar{q}\cosh 2\Xi}}
\end{aligned}$$

for any $p_1 > 0$ and $q_1 \geq 0$, where $\varepsilon = \frac{\bar{q}\sinh 2\Xi_L}{\sqrt{\alpha+2\bar{q}\cosh 2\Xi_L}}L + O\left(\frac{1}{\alpha+2\bar{q}\cosh 2(\Xi+L)}\right)$.

Similarly, we obtain

$$|\rho_2 - \rho_2^{app}| = O\left((\alpha+2\bar{q}\cosh 2\Xi)^{-\frac{3}{2}}\right), \text{ for } \alpha \text{ large.}$$

For the overlapping case, $L > 0$, we make the ansatz that the eigenvalues α have the leading asymptotic term $\alpha = CL^{-\gamma}$ for a given $\gamma \in (0,1)$. Then we find that $|\rho_1 - \rho_1^{app}| = O(L^{1+\gamma})$ and $|\rho_2 - \rho_2^{app}| = O(L^{\frac{3}{2}\gamma})$ as L tends to zero. We also obtain simply by a Taylor expansion that $|\rho_{cla} - \rho_{cla}^{app}| = \left|\rho_{cla} - e^{-2\sqrt{\alpha+2\bar{q}\cosh 2\Xi}L}\right| = O\left(L^{1-\frac{\gamma}{2}}\right)$ for L small. When there is no overlap, $L = 0$, we find that both $|\rho_1 - \rho_1^{app}|$ and $|\rho_2 - \rho_2^{app}|$ behave like $O\left((\alpha+2\bar{q}\cosh 2\Xi)^{-\frac{3}{2}}\right)$ for α large.

In summary, we obtain for the overlapping case when L is small

$$\begin{aligned}
|\rho - \rho_{app}| &\leq |\rho_1 - \rho_1^{app}|\,|\rho_2 \cdot \rho_{cla}| + |\rho_2 - \rho_2^{app}|\,|\rho_1^{app} \cdot \rho_{cla}| \\
&\quad + |\rho_{cla} - \rho_{cla}^{app}|\,|\rho_1^{app} \cdot \rho_2^{app}| \\
&= O\left(L^{\min(1-\frac{\gamma}{2}, \frac{3}{2}\gamma)}\right)
\end{aligned}$$

by noting that each term of $|\rho_2|, |\rho_{cla}|, |\rho_1^{app}|$ and $|\rho_2^{app}|$ is bounded by one. For the nonoverlapping case the result can be obtained similarly. □

We show in Figure 2 a comparison of the exact and approximate convergence factor for two examples, using $\eta = 2$, $f = 1$, $L = 0.01$, and on the left $\Xi = 0.5$, and on the right $\Xi = 0.1$. We see that for large eigenvalues, ρ_{app} approximates ρ very well, but for small eigenvalues we see large deviations, especially when the domain parameter Ξ is small.

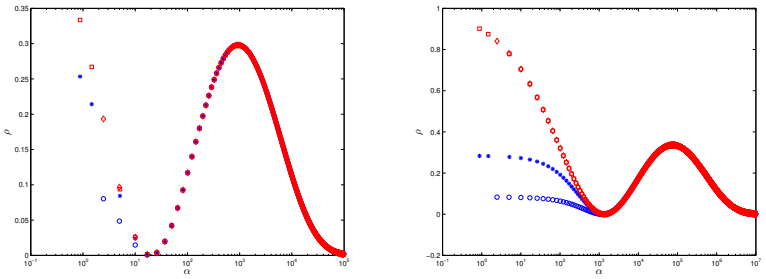

Fig. 2 The convergence factor ρ (blue stars and circles) compared with its approximation ρ_{app} (red squares and diamonds) with $p_1 = p_2$ given by (41) and $q_1 = q_2 = 0$, where $\eta = 2, f = 1$. For the left plot $\Xi = 0.5$, $\bar{\Xi} = 1$, $L = 0.01$, and for the right plot $\Xi = 0.05$, $\bar{\Xi} = 0.1$, $L = 0.001$. The stars and squares represent values at even mode eigenvalues and the circles and diamonds represent values at odd mode eigenvalues. Note that we have added the constant 1 to the eigenvalues α to avoid logarithmic values of negative numbers.

3.1 Taylor transmission conditions

From the proof of Theorem 1, we see that the classical Schwarz method can only damp efficiently the errors for large eigenvalues of (11), but not for small eigenvalues, which is typical for classical Schwarz methods, see [16,24,28,26]. A simple remedy for this is to use a low frequency approximation of the optimal $\sigma_i(\alpha)$ using a Taylor expansion to determine the free parameters occurring in (30). Instead of expanding at zero as in [16], we expand the optimal $\sigma_i(\alpha)$ at the smallest eigenvalue $\alpha = \alpha_{\min}$ [26] and find

$$\begin{aligned}\sigma_1(\alpha) &= v_{\alpha_{\min}}(\Xi + L) + O(\alpha - \alpha_{\min}),\\ \sigma_2(\alpha) &= -w_{\alpha_{\min}}(\Xi) + O(\alpha - \alpha_{\min}),\end{aligned}$$

which implies that we should choose $p_1 = v_{\alpha_{\min}}(\Xi + L)$, $p_2 = w_{\alpha_{\min}}(\Xi)$ and $q_1 = q_2 = 0$ to obtain a so-called Taylor transmission condition of order 0 (T0). We denote by $\rho_{T0}(\alpha, \Xi, L, p_1, p_2)$ the corresponding convergence factor. In theory, we could also use a higher order Taylor expansion of $\sigma_i(\alpha)$ in α to obtain higher order transmission conditions, but the expressions of the functions w_α and v_α are not easy to handle, and it is hard to get the corresponding theoretical result.

Theorem 3 (Taylor asymptotics) *When there is overlap, $L > 0$, we have for the zeroth order Taylor approximation T0 for L small the asymptotic convergence factor estimate*

$$\max_{\alpha\in\mathbb{E}} \rho_{T0}(\alpha, \Xi, L, v_{\alpha_{\min}}(\Xi + L), w_{\alpha_{\min}}(\Xi)) = 1 - 4G_{\min}^{\frac{1}{2}} L^{\frac{1}{2}} + O(L). \tag{38}$$

When there is no overlap, $L = 0$, we have for $\alpha_{\max}$ large the asymptotic convergence factor estimate

$$\max_{\alpha\in\mathbb{E}_N} \rho_{T0}(\alpha, \Xi, 0, v_{\alpha_{\min}}(\Xi), w_{\alpha_{\min}}(\Xi)) = 1 - 2G_{\min}\alpha_{\max}^{-\frac{1}{2}} + O(\alpha_{\max}^{-1}). \tag{39}$$

Proof Consider first the overlapping case $L > 0$. Similar to the technique applied in Theorem 3.4 in [16], it is not hard to show that the convergence factor $\rho_{app}(\alpha, \Xi, L, v_{\alpha_{\min}}(\Xi + L), w_{\alpha_{\min}}(\Xi), 0, 0)$ attains its interior maximum at $\alpha_{T0} \sim G_{\min} L^{-1}$ for L small. Inserting α_{T0} into $\rho_{app}(\alpha, \Xi, L, v_{\alpha_{\min}}(\Xi + L), w_{\alpha_{\min}}(\Xi), 0, 0)$ and expanding in L for L small gives $\rho_{app}(\alpha_{T0}, \Xi, L, v_{\alpha_{\min}}(\Xi + L), w_{\alpha_{\min}}(\Xi), 0, 0) = 1 - 4G_{\min}^{\frac{1}{2}} L^{\frac{1}{2}} + O(L)$. We next consider the nonoverlapping case, $L = 0$. From Lemmas 5 and 6, it is not hard to show that the convergence factor $\rho_{T0}(\alpha, \Xi, 0, v_{\alpha_{\min}}(\Xi), w_{\alpha_{\min}}(\Xi))$ is monotonically increasing in α and thus attains its maximum at $\alpha_{\max}$. A series expansion with respect to $\alpha_{\max}$ for $\alpha_{\max}$ large then gives the desired result. □

3.2 Optimized transmission conditions

In this subsection we study the following classes of optimized transmission conditions:

OO0 (Optimized of Order 0): $p_i = p > 0, q_i = 0, i = 1, 2$;
OO2 (Optimized of Order 2): $p_i = p > 0, q_i = q > 0, i = 1, 2$;
O2s (Optimized 2 sided): $p_i > 0, q_i = 0, i = 1, 2$.

For each case, we need to solve the following min-max problem to determine the free parameters involved:

$$\min_{p_i, q_i \in O_c} \max_{\alpha \in \tilde{\mathbb{E}}} \left| \rho(\alpha, \Xi, L, p_1, p_2, q_1, q_2) \right|, \tag{40}$$

where $\tilde{\mathbb{E}} = \mathbb{E}$ for the overlapping case $L > 0$ and $\tilde{\mathbb{E}} = \mathbb{E}_N$ for the nonoverlapping case $L = 0$ and O_c is one of the classes of transmission conditions OO0, OO2, or O2s. The solution of the optimization problem (40) gives for the case OO0 the optimized transmission conditions of order 0 (also known as optimized Robin transmission conditions), for the case OO2 the optimized transmission conditions of order 2 (also known as optimized Ventcell transmission condition) and for the case O2s the optimized two-sided Robin transmission conditions.

As we have already mentioned, solving the min-max problems (40) involving the Mathieu like functions and their derivatives is not an easy task. To our best knowledge, the min-max problem (40) cannot be transformed into any problem that is well studied. However, with the monotonicity results proved in Lemmas 5 and 6, we can apply the techniques used in [24,28], that is when the eigenvalue α is small we use the convergence factor ρ itself but when α is large we use the approximate convergence factor ρ_{app}, to determine asymptotic solutions to the optimization problem (40). For simplicity of this presentation, we omit the details for solving (40) and just present the corresponding results in the following theorems.

Theorem 4 (OO0) *Assume that the OO0 transmission conditions are used. For the overlapping case, $L > 0$, the asymptotically optimal parameter choice*

solving the min-max problem (40) is

$$p^* = 2^{-1} G_{\min}^{\frac{2}{3}} L^{-\frac{1}{3}}. \tag{41}$$

The parameter p^* is the unique asymptotic solution of the equi-oscillation equation

$$\rho(\alpha_{\min}, \Xi, L, p^*, p^*, 0, 0) = \rho(\alpha^*, \Xi, L, p^*, p^*, 0, 0), \tag{42}$$

where $\alpha^* \sim G_{\min}^{\frac{2}{3}} L^{-\frac{4}{3}}$ is the unique interior maximum point of $\rho_{app}(\alpha, \Xi, L, p^*, p^*, 0, 0)$. With the choice p^* we obtain with overlap $L > 0$ small the convergence factor estimate

$$\max_{\alpha \in \mathbb{E}} |\rho(\alpha, \Xi, L, p^*, p^*, 0, 0)| = 1 - 4 G_{\min}^{\frac{1}{3}} L^{\frac{1}{3}} + O(L^{\frac{2}{3}}). \tag{43}$$

For the nonoverlapping case, $L = 0$, let $v_{\min} := v_{\alpha_{\min}}(\Xi)$, $w_{\min} := w_{\alpha_{\min}}(\Xi)$ and $v_{\max}$, $w_{\max}$ be similarly defined. Then the optimal parameter choice solving the min-max problem (40) is

$$\hat{p} = \left(\frac{v_{\max} v_{\min}(w_{\max} - w_{\min}) + w_{\max} w_{\min}(v_{\max} - v_{\min})}{v_{\max} - v_{\min} + w_{\max} - w_{\min}} \right)^{\frac{1}{2}}. \tag{44}$$

The parameter $\hat{p}$ is uniquely determined by the equi-oscillation equation

$$\rho(\alpha_{\min}, \Xi, 0, \hat{p}, \hat{p}, 0, 0) = \rho(\alpha_{\max}, \Xi, 0, \hat{p}, \hat{p}, 0, 0), \tag{45}$$

and behaves like $\hat{p} \sim 2^{-\frac{1}{2}} G_{\min}^{\frac{1}{2}} \alpha_{\max}^{\frac{1}{4}}$ for $\alpha_{\max}$ large, which leads to the convergence factor estimate

$$\max_{\alpha \in \mathbb{E}_N} |\rho(\alpha, \Xi, 0, \hat{p}, \hat{p}, 0, 0)| = 1 - 2^{\frac{3}{2}} G_{\min}^{\frac{1}{2}} \alpha_{\max}^{-\frac{1}{4}} + O(\alpha_{\max}^{-\frac{1}{2}}). \tag{46}$$

Theorem 5 (OO2) *Assume that the OO2 transmission conditions are used. For the overlapping case, $L > 0$, the asymptotically optimal parameter choice solving the min-max problem (40) for $L > 0$ small is*

$$p^* = 2^{-\frac{7}{5}} G_{\min}^{\frac{4}{5}} L^{-\frac{1}{5}}, \quad q^* = 2^{\frac{1}{5}} G_{\min}^{-\frac{2}{5}} L^{\frac{3}{5}}. \tag{47}$$

The parameters p^*, q^* are the asymptotic solutions of the equi-oscillation equations

$$\rho(\alpha_{\min}, \Xi, L, p^*, p^*, q^*, q^*) = \rho(\alpha_1^*, \Xi, L, p^*, p^*, q^*, q^*) = \rho(\alpha_2^*, \Xi, L, p^*, p^*, q^*, q^*) \tag{48}$$

with $\alpha_1^* \sim 2^{-\frac{8}{5}} G_{\min}^{\frac{6}{5}} L^{-\frac{4}{5}}$ and $\alpha_2^* \sim 2^{\frac{4}{5}} G_{\min}^{\frac{2}{5}} L^{-\frac{8}{5}}$ the interior maximum points of $\rho_{app}(\alpha, \Xi, L, p^*, p^*, q^*, q^*)$. With the choice p^*, q^*, we obtain with overlap $L > 0$ small the convergence factor estimate

$$\max_{\alpha \in \mathbb{E}} |\rho(\alpha, \Xi, L, p^*, p^*, q^*, q^*)| = 1 - 2^{\frac{12}{5}} G_{\min}^{\frac{1}{5}} L^{\frac{1}{5}} + O(L^{\frac{2}{5}}). \tag{49}$$

For the nonoverlapping case, $L = 0$, the asymptotically optimal parameter choice solving the min-max problem (40) for $\alpha_{\max}$ large is

$$\hat{p} = 2^{-\frac{5}{4}} G_{\min}^{\frac{3}{4}} \alpha_{\max}^{\frac{1}{8}}, \quad \hat{q} = 2^{-\frac{1}{4}} G_{\min}^{-\frac{1}{4}} \alpha_{\max}^{-\frac{3}{8}}. \tag{50}$$

These parameters are uniquely determined as asymptotic solutions of the equi-oscillation equations

$$\rho(\alpha_{\min}, \Xi, 0, \hat{p}, \hat{p}, \hat{q}, \hat{q}) = \rho(\hat{\alpha}, \Xi, 0, \hat{p}, \hat{p}, \hat{q}, \hat{q}) = \rho(\alpha_{\max}, \Xi, 0, \hat{p}, \hat{p}, \hat{q}, \hat{q}) \tag{51}$$

with $\hat{\alpha} = \frac{\hat{p}}{\hat{q}} - 4\bar{q}\cosh 2\Xi$. This asymptotically optimal choice leads to the convergence factor estimate

$$\max_{\alpha \in \mathbb{E}_N} |\rho(\alpha, \Xi, 0, \hat{p}, \hat{p}, \hat{q}, \hat{q})| = 1 - 2^{\frac{9}{4}} G_{\min}^{\frac{1}{4}} \alpha_{\max}^{-\frac{1}{8}} + O(\alpha_{\max}^{-\frac{1}{4}}). \tag{52}$$

Theorem 6 (O2s) *Assume that the O2s transmission conditions are used. For the overlapping case, $L > 0$, the asymptotically optimal parameter choice solving the min-max problem (40) for $L > 0$ small is*

$$p_1^* = 2^{-\frac{8}{5}} G_{\min}^{\frac{4}{5}} L^{-\frac{1}{5}}, \quad p_2^* = 2^{-\frac{4}{5}} G_{\min}^{\frac{2}{5}} L^{-\frac{3}{5}}. \tag{53}$$

The parameters p_1^*, p_2^* solve asymptotically the equi-oscillation equations

$$\rho(\alpha_{\min}, \Xi, L, p_1^*, p_2^*, 0, 0) = -\rho(\bar{\alpha}_1, \Xi, L, p_1^*, p_2^*, 0, 0) = \rho(\bar{\alpha}_2, \Xi, L, p_1^*, p_2^*, 0, 0), \tag{54}$$

where $\bar{\alpha}_1 \sim 2^{-\frac{12}{5}} G_{\min}^{\frac{6}{5}} L^{-\frac{4}{5}}$ is the interior minimum point and $\bar{\alpha}_2 \sim 2^{-\frac{4}{5}} G_{\min}^{\frac{2}{5}} L^{-\frac{8}{5}}$ is the interior maximum point of $\rho_{app}(\alpha, \Xi, L, p_1^*, p_2^*, 0, 0)$. With the choice p_1^*, p_2^*, we obtain with overlap $L > 0$ small the convergence factor estimate

$$\max_{\alpha \in \mathbb{E}} |\rho(\alpha, \Xi, L, p_1^*, p_2^*, 0, 0)| = 1 - 2^{\frac{8}{5}} G_{\min}^{\frac{1}{5}} L^{\frac{1}{5}} + O(L^{\frac{2}{5}}). \tag{55}$$

For the nonoverlapping case, $L = 0$, the asymptotically optimal parameter choice solving the min-max problem (40) for $\alpha_{\max}$ large is

$$\hat{p}_1 = 2^{-\frac{5}{4}} G_{\min}^{\frac{3}{4}} \alpha_{\max}^{\frac{1}{8}}, \quad \hat{p}_2 = 2^{\frac{1}{4}} G_{\min}^{\frac{1}{4}} \alpha_{\max}^{\frac{3}{8}}. \tag{56}$$

These parameters are uniquely determined as asymptotic solutions of the equi-oscillation equations

$$\rho(\alpha_{\min}, \Xi, 0, \hat{p}_1, \hat{p}_2, 0, 0) = -\rho(\underline{\alpha}, \Xi, 0, \hat{p}_1, \hat{p}_2, 0, 0) = \rho(\alpha_{\max}, \Xi, 0, \hat{p}_1, \hat{p}_2, 0, 0), \tag{57}$$

with $\underline{\alpha} = \hat{p}_1 \hat{p}_2 - 2\bar{q}\cosh 2\Xi$. This asymptotically optimal choice leads to the convergence factor estimate

$$\max_{\alpha \in \mathbb{E}_N} |\rho(\alpha, \Xi, L, \hat{p}_1, \hat{p}_2, 0, 0)| = 1 - 2^{\frac{5}{4}} G_{\min}^{\frac{1}{4}} \alpha_{\max}^{-\frac{1}{8}} + O(\alpha_{\max}^{-\frac{1}{4}}). \tag{58}$$

4 Further discussion

We now show how our results can be used to recover results in the literature as special cases, and in doing so discover an interesting common form of these asymptotically optimized transmission conditions, which leads to four different ways to determine approximately optimized transmission conditions. We then discuss implementation issues, and also give a generalization for variable coefficients using the techniques we developed for elliptical domain decomposition.

4.1 Uniform results for OSMs

Our results in the previous section showed that the constant $G_{\min}:= w_{\alpha_{\min}}(\Xi) - v_{\alpha_{\min}}(\Xi)$, which depends on the model parameter η and the interface parameters f and Ξ, enters the optimized transmission parameters and the corresponding convergence rate estimates. If we set instead $G_{\min}:= \sqrt{\eta}\left(\frac{I'_{k_{\min}}(\sqrt{\eta}R)}{I_{k_{\min}}(\sqrt{\eta}R)} - \frac{K'_{k_{\min}}(\sqrt{\eta}R)}{K_{k_{\min}}(\sqrt{\eta}R)}\right)$ in our analysis, we recover all the results of the optimized transmission parameters and the corresponding asymptotic estimates for circular domain decompositions from [24,28] in both the overlapping and nonoverlapping cases. Here $I_k(x)$ and $K_k(x)$ are the modified Bessel functions of the first and the second kind, and R is the radius of the circular interface. Furthermore, if we set $G_{\min}:= 2\sqrt{\alpha_{\min}}$, we also recover from our results all the results of OSMs for model problems with variable reaction term [26], where $\alpha_{\min}$ is the smallest eigenvalue of an interface Sturm-Liouville problem involving the variable coefficient. In addition, if set $G_{\min}:= \sqrt{k^2+\eta}\left(\coth(\sqrt{k^2+\eta}a) + \coth(\sqrt{k^2+\eta}b)\right)$, we recover from our results all the results of optimized Schwarz methods for bounded domain decomposition [48], where a and b, which are different from our context, are subdomain geometry parameters. And if we finally set $G_{\min}:= 2\sqrt{k_{\min}^2+\eta}$, we recover the original results for domain decompositions with straight interfaces [16].

It was shown in [28] that by a natural scaling k/R of the Fourier frequencies, one can well approximate optimized transmission conditions for circular domain decompositions from the original straight interface analysis in [16]. This result suggests a local scaling by interface curvature for domain decompositions with general curved interfaces, which is of course applicable to our elliptical domain decomposition. We can also take a different viewpoint that accounts for the natural scaling k/R, namely optimizing the approximate convergence factor ρ_{app} directly. In doing so, we find the same formulas for optimized transmission parameters and corresponding asymptotic estimates of the convergence rate, except that $G_{\min}$ should be replaced by $G_{\min}^{app}:= 2\sqrt{\alpha_{\min}+2\bar{q}\cosh 2\bar{\Xi}}$.

The discussion above shows that the function $G(\alpha,\Xi)$ plays a key role in determining the optimized transmission conditions. Since the function G

consists of functions determined by ordinary differential equations, no built-in routine can calculate it except in special cases. We thus now show how to evaluate such functions numerically, using the following three steps for a given $L > 0$ small:

Step 1: Solve (numerically if needed) the differential equation (10) for $\alpha := \alpha_{\min}$ with the boundary conditions

$$\begin{aligned} R'_{\alpha_{\min}}(0) = 0,\ R_{\alpha_{\min}}(\Xi + L) = 1, \qquad &\text{when} \quad \alpha_{\min} \in \mathbb{E}_e, \\ R_{\alpha_{\min}}(0) = 0,\ R_{\alpha_{\min}}(\Xi + L) = 1, \qquad &\text{when} \quad \alpha_{\min} \in \mathbb{E}_o, \end{aligned}$$

and denote the corresponding solution by $R_l(\xi)$.

Step 2: Solve the same differential equation (10) for $\alpha := \alpha_{\min}$ with the boundary conditions

$$R_{\alpha_{\min}}(\Xi) = R_l(\Xi),\ R_{\alpha_{\min}}(\bar{\Xi}) = 0,$$

and denote the corresponding solution by $R_r(\xi)$.

Step 3: Set $G_{\min} := (1 - R_r(\Xi + L))/L$.

With this approach, we only need to know the smallest eigenvalue $\alpha_{\min}$ of (11), which can be estimated numerically in many ways, see for example [37] for a finite difference approximation and [26] for a Fourier spectral approximation. In our case, this value is available in Maple. In addition, it is with this procedure not necessary to calculate the derivatives occurring in the formula for $G(\alpha_0^e, \Xi)$.

Remark 2 This strategy for determining $G_{\min}$ also works for other boundary conditions than Dirichlet, one only needs to modify the condition $R_{\alpha_{\min}}(\bar{\Xi}) = 0$ in Step 2 correspondingly. In addition, it is applicable for straight interface analysis [16], for circular domain decompositions [24,28] and for finite domain decompositions [48] as well and can lead to better performance, since it can take into account the subdomain geometry, which in certain circumstances can affect notably the performance of Schwarz iterations, see [48].

We thus have now the following four strategies for determining $G_{\min}$ in the OSMs:

S1 : Evaluating $G_{\min}$ directly by computing the solutions and their derivatives of the BVP problems (14,16) and (15).
S2 : Using $G_{\min}$ calculated by the above-mentioned 3-step procedure.
S3 : Using $G_{\min}^{app} = 2\sqrt{\alpha_{\min} + 2\bar{q}\cosh 2\bar{\Xi}}$ as an approximation of $G_{\min}$.
S4 : Using the optimized transmission parameters from the straight interface analysis [16] scaled locally by interface curvature.

We note here that the first three strategies require the smallest eigenvalue $\alpha_{\min}$, while the last strategy S4 does not, which of course simplifies its application.

4.2 Implementation issues

Our analysis showed that the optimized parameters are constants along the interface in the elliptic coordinates, which would simplify the implementation of the OSMs in elliptic coordinates. However, since the even and odd modes satisfy different boundary conditions, it is not easy to run the the Schwarz iteration process in elliptic coordinates, since the errors in both modes will occur. Thus, except for annular or annular sector domain problems, one would still run the algorithm in Cartesian coordinates, which can also reduce the number of unknowns. We thus give now some useful relations between the Cartesian coordinates (x, y) and the elliptic coordinates (ξ, θ) and explain the implementation in Cartesian coordinates in more detail.

Denoting by $a := f\cosh\xi$ and $b := f\sinh\xi$, a direct calculation shows that $\frac{\partial u}{\partial n} = \frac{1}{h_\xi}\frac{\partial u}{\partial \xi}$ and $\frac{\partial u}{\partial \tau} = \frac{1}{h_\xi}\frac{\partial u}{\partial \theta}$, where $\frac{\partial}{\partial \tau}$ represents the tangential derivative on the interfaces and $h_\xi = f\sqrt{\cosh^2\xi - \cos^2\theta} = \sqrt{a^2 - f^2\cos^2\theta} = \sqrt{a^2\sin^2\theta + b^2\cos^2\theta}$. When implemented in Cartesian coordinates, one uses normal derivatives and not derivatives along the ξ-direction, and we see that the optimized transmission parameters have to be scaled by the factor $\frac{1}{h_\xi}$. Hence, in the Cartesian coordinates, the optimized transmission parameters are variable and depend on the angle θ. The following formulas of h_ξ in the Cartesian variables (x, y) simplify the implementation:

$$\begin{aligned} h_\xi &= \sqrt{a^2\sin^2\theta + b^2\cos^2\theta} = \sqrt{\frac{y^2 f^2\cosh^2\xi}{f^2\sinh^2\xi} + \frac{x^2 f^2\sinh^2\xi}{f^2\cosh^2\xi}} \\ &= \sqrt{x^2\tanh^2\xi + y^2\coth^2\xi}. \end{aligned} \tag{59}$$

Assuming that a uniform mesh on the interface with mesh size h is used in Cartesian coordinates, we now derive the corresponding angular mesh size h_θ. For two adjacent nodes on the ellipse given by $A = A(a\cos\theta, b\sin\theta)$, $B = B(a\cos(\theta + h_\theta), b\sin(\theta + h_\theta))$, the distance between A and B is given by

$$\begin{aligned} h &= \sqrt{a^2(\cos(\theta + h_\theta) - \cos\theta)^2 + b^2(\sin(\theta + h_\theta) - \sin\theta)^2} \\ &= \sqrt{a^2(-h_\theta\sin\theta + \ldots)^2 + b^2(h_\theta\cos\theta + \ldots)^2} \\ &\approx \sqrt{a^2\sin^2\theta h_\theta^2 + b^2\cos^2\theta h_\theta^2} \\ &= h_\xi h_\theta, \end{aligned}$$

where we used a Taylor expansion and neglected higher order terms. Finally, the curvature on the ellipse is given by $\kappa = \frac{ab}{h_\xi^3}$, which is useful when implementing the strategy S4.

4.3 Analysis of the approximation strategies S3 and S4

While the strategy S1 which comes directly from our analysis, and S2 which can be justified using a Taylor expansion, are efficient, we now analyze the

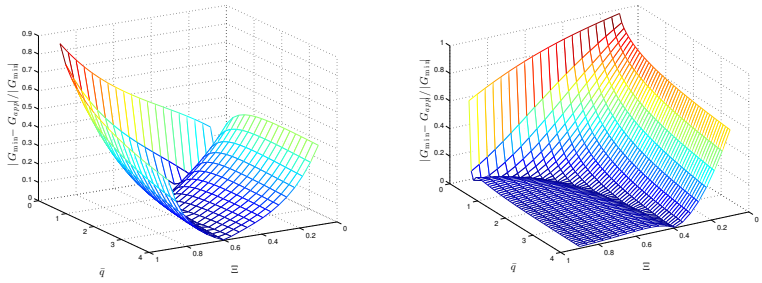

Fig. 3 Relative difference between $G_{\min}$ and $G_{\min}^{app}$ as a function of Ξ and $\bar{q}$. On the left for $\bar{\Xi} = 1$ fixed and on the right for $\bar{\Xi} = 2\Xi$.

approximation strategies S3 and S4 in more detail. For S3, we plot on the left in Figure 3 the relative difference between $G_{\min}$ and $G_{\min}^{app}$ as a function of $\bar{q}$ and Ξ with $\bar{\Xi} = 1$. We see that for all $\bar{q}$ and Ξ the quantity $G_{\min}^{app}$ is not a bad approximation to $G_{\min}$, since the relative difference is bounded by 1. We also clearly see a curve in the $(\Xi, \bar{q})$ plane on which $G_{\min}^{app}$ is a very good approximation of $G_{\min}$. This shows that it would be possible to choose the position of the interfaces for fixed $\bar{q}$ to make the strategy S3 more efficient, which is however not a viable approach in practice under the constraint of load balancing. We see however that for large $\bar{q}$ (this means η large for a fixed computational domain), balancing the subdomain sizes is good for S3. On the right in Figure 3 we show the case where the boundary of the domain is chosen as $\bar{\Xi} = 2\Xi$, which means that the subdomain sizes are balanced. In both plots we find that when $\bar{q}$ decreases to zero (that is the parameter η goes to zero for fixed confocal distance $2f$), $G_{\min}^{app}$ can not approximate $G_{\min}$ very well. This is due to the fact that η plays the role of a regularization parameter, and when η is small, $G_{\min}^{app}$ cannot catch the fine details of $G_{\min}$. Another observation is that for decreasing Ξ, the relative difference increases, which means for flat and elongated ellipses, the approximation $G_{\min}^{app}$ deteriorates. To see this more clearly, we plot in Figure 4 the convergence factor with the optimized transmission parameter given in (41) using this new approximation $G_{\min}^{app}$. Comparing with Figure 2 we see that, for a fairly round domain (left plots in Figures 2 and 4 with $\Xi = 0.5, \bar{\Xi} = 1, L = 0.01$) both $G_{\min}$ and $G_{\min}^{app}$ lead to almost the same maximum values of the convergence factor ρ; however, for flat and elongated domains (right plots in Figures 2 and 4 with $\Xi = 0.05, \bar{\Xi} = 0.1, L = 0.001$) the maximum value of the convergence factor ρ determined by $G_{\min}^{app}$ is more than twice the one determined by $G_{\min}$. This can be explained as follows: introducing in the Mathieu differential equation

$$R''_{\xi\xi} - (\alpha_k + \frac{f^2\eta}{2}\cosh 2\xi)R = 0$$

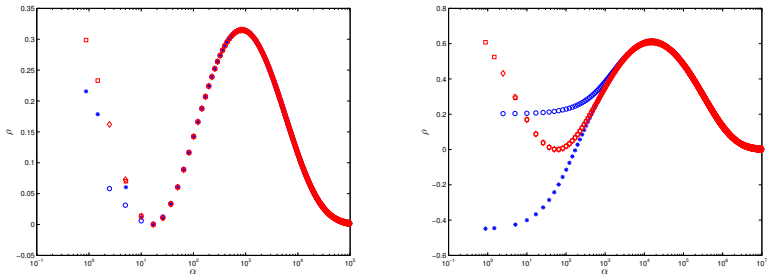

Fig. 4 The convergence factor ρ (blue stars and circles) compared to its approximation ρ_{app} (red squares and diamonds), where $\eta = 2$, $f = 1$, $q_1 = q_2 = 0$, and $p_1 = p_2$ are determined by (41) with $G_{\min}$ being replaced by $G_{\min}^{app}$. For the left plot $\Xi = 0.5$, $\bar{\Xi} = 1$, $L = 0.01$, and for the right plot $\Xi = 0.05$, $\bar{\Xi} = 0.1$, $L = 0.001$. The stars and squares represent values at even mode eigenvalues and the circles and diamonds represent values at odd mode eigenvalues. Note again that we have added the constant 1 to the eigenvalues α to avoid logarithmic values of negative numbers.

the change of variables $r = \frac{fe^{\xi}}{2}$, we get

$$R_{rr}^{''} + \frac{R_r^{'}}{r} - (\frac{\alpha_k}{r^2} + \eta(1 + e^{-4\xi}))R = 0.$$

Thus, the solution $R_{\alpha_k}(\xi)$ tends to the modified Bessel function $K_k(\sqrt{\eta}r)$ or $I_k(\sqrt{\eta}r)$ (depending on the monotonicity) as $\xi \to \infty$ and $f \to 0$, since α_k tends to k^2 by Lemma 1. Therefore, when $\xi \to \infty$ and $f \to 0$, $G_{\min}^{app}$ tends to $2\sqrt{k_{\min}^2 + \eta\tilde{R}^2}$, where $k_{\min}$ is the smallest angular wise frequency involved in the circular domain decomposition and $\tilde{R}$ is the radius of the corresponding interface. Since for circular domain decomposition it has been shown in [28] that the term $2\sqrt{k_{\min}^2 + \eta\tilde{R}^2}$ is a good approximation to the corresponding $G_{\min}$, we can then expect for elliptical domain decomposition that $G_{\min}^{app}$ provides a fairly good approximation to $G_{\min}$, provided that the ellipse is not too flat.

We next investigate the strategy S4 for the nonoverlapping OO0 case; the other cases can be analyzed similarly. The optimized Robin parameter $\tilde{p}$ from the straight interface analysis in [16] is given by

$$\tilde{p} = (k_{\min,l}^2 + \eta)^{\frac{1}{4}} k_{\max,l}^{\frac{1}{2}}, \tag{60}$$

where $k_{\min,l}$ and $k_{\max,l}$ represent the lowest and the highest Fourier frequencies involved in the calculation. Since in our case in the θ direction the boundary condition is periodic, we have $k_{\min,l} = 0$, and $k_{\max}$ can be estimated by π/h with h being the mesh size along the interface. If one does not know from which geometry the curved interface comes, i.e. one does not know it is an ellipse, one would like to estimate the angular mesh size as $h_\theta \approx h\kappa$ with κ being the

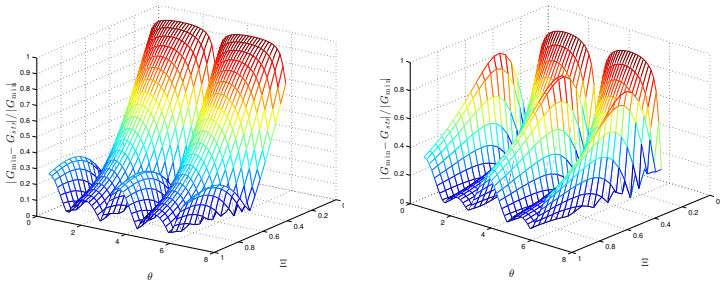

Fig. 5 Relative differences between $G_{\min}$ and G_{str} as a function of θ and Ξ. The left plot is for $\eta = 2$, $f = 1$ and the right plot is for $\eta = 20$, $f = 1$.

local curvature of the curved interface. This leads to $\tilde{p} \approx \eta^{\frac{1}{4}} \pi^{\frac{1}{2}} h_\theta^{-\frac{1}{2}} \kappa^{\frac{1}{2}}$, and inserting $\kappa = \frac{ab}{h_\xi^3}$ we get

$$\tilde{p} \approx \eta^{\frac{1}{4}} \frac{a^{\frac{1}{2}} b^{\frac{1}{2}}}{h_\xi^{\frac{3}{2}}} \frac{\pi^{\frac{1}{2}}}{h_\theta^{\frac{1}{2}}}.$$

We now consider the optimized Robin transmission parameter $\hat{p} = 2^{-\frac{1}{2}} G_{\min}^{\frac{1}{2}} \alpha_{\max}^{\frac{1}{4}}$ given in Theorem 4. If we use in Cartesian coordinates the normal derivative in the Robin transmission conditions, the transmission parameter becomes

$$\hat{p}_n = \frac{1}{h_\xi} \hat{p} = \frac{1}{h_\xi} 2^{-\frac{1}{2}} G_{\min}^{\frac{1}{2}} \frac{\pi^{\frac{1}{2}}}{h_\theta^{\frac{1}{2}}},$$

where we inserted the estimate $\alpha_{\max} \approx \pi^2 / h_\theta^2$. To compare $\tilde{p}$ and $\hat{p}_n$, we need to investigate the difference between $G_{\min}$ and $2\sqrt{\eta} \frac{ab}{\sqrt{a^2 \sin^2\theta + b^2 \cos^2\theta}} =: G_{str}$, where we have used the expression of h_ξ given in (59)[1]. In Figure 5 we show the relative difference between $G_{\min}$ and G_{str} as a function of Ξ and θ with $\bar{\Xi} = 2\Xi$, on the left for $f = 1, \eta = 2$ and on the right for $f = 1, \eta = 20$. We see that the relative difference is bounded by 1 and grows as Ξ goes to zero, which again corresponds to the case where the interface becomes a more and more flat ellipse. In addition, unlike in the approximation $G_{\min}^{app}$, larger η does not mean a better approximation.

4.4 Applications to model problems with variable coefficients

We now show that our analysis also applies to the case of a general diffusion reaction model with variable coefficients of the form

$$\begin{aligned} -\nabla \cdot (a(x,y) \nabla u(x,y)) + \eta(x,y) u(x,y) &= g(x,y) \text{ in } \Omega, \\ \mathcal{B} u(x,y) &= 0 \qquad \text{on } \partial\Omega, \end{aligned} \tag{61}$$

[1] Here we neglect the fact that when the ellipse is angular-wise uniformly meshed with mesh size h_θ, the interface is not correspondingly uniformly meshed anymore.

where the domain is a rectangle, $\Omega = (-\underline{c}, \bar{d}) \times (0,1)$, and $\mathcal{B}u = 0$ denotes certain boundary conditions, for example homogeneous Dirichlet conditions. The function $a(x,y)$ is positive with smooth derivatives and $\eta(x,y)$ is positive. When $\eta(x,y)$ depends only on y and the diffusion coefficient $a(x,y) \equiv 1$, OSMs were systematically analyzed in [26] by using the technique of separation of variables. We now show that our analysis here can be extended to the case where

$$a(x,y) = a_1(x)a_2(y) \quad \text{and} \quad \eta(x,y) = c_1\eta_1(x)a_2(y) + c_2\eta_2(y)a_1(x), \tag{62}$$

with the two subdomains $\Omega_1 = (-\underline{c}, L) \times (0,1)$ and $\Omega_2 = (0, \bar{d}) \times (0,1)$, where $L > 0$ describes the overlap. An optimized parallel Schwarz method for (61) is

$$\begin{aligned} -\nabla \cdot (a(x,y)\nabla u_1^n(x,y)) + \eta(x,y)u_1^n(x,y) &= g(x,y) \text{ in } \Omega_1, \\ \mathcal{B}u_1^n(x,y) &= 0 \qquad \text{on } \partial\Omega_1 \cap \partial\Omega, \\ -\nabla \cdot (a(x,y)\nabla u_2^n(x,y)) + \eta(x,y)u_2^n(x,y) &= g(x,y) \text{ in } \Omega, \\ \mathcal{B}u_2^n(x,y) &= 0 \qquad \text{on } \partial\Omega_2 \cap \partial\Omega, \end{aligned}$$

with the transmission conditions

$$a(L,y)\frac{\partial u_1^n}{\partial x}(L,y) + \mathcal{S}_1 u_1^n(L,y) = a(L,y)\frac{\partial u_2^{n-1}}{\partial x}(L,y) + \mathcal{S}_1 u_2^{n-1}(L,y), \tag{63}$$

$$a(0,y)\frac{\partial u_2^n}{\partial x}(0,y) - \mathcal{S}_2 u_2^n(0,y) = a(0,y)\frac{\partial u_1^{n-1}}{\partial x}(0,y) - \mathcal{S}_2 u_1^{n-1}(0,y). \tag{64}$$

As before, we only need to study the error equation, $g = 0$. Following the approach for elliptical domain decomposition, we make the ansatz that the subdomain solutions at each iteration are variable separable, $u_i^n(x,y) = R_i^n(x)\Phi(y)$, and find that the subdomain solutions can be decoupled into the following ODE problems: the Sturm-Liouville eigenvalue problem

$$(a_2(y)\Phi'(y))' + (\alpha a_2(y) - c_2\eta_2(y))\Phi(y) = 0, \quad \Phi(0) = \Phi(1) = 0, \tag{65}$$

and the second order ODE corresponding to the subdomain problems

$$(a_1(x)(R_i^n)'(x))' - (\alpha a_1(x) + c_1\eta_1(x))R_i^n(x) = 0,$$

with boundary conditions determined by the subdomain problems. It is well known that there is an infinite number of positive, separated eigenvalues $\alpha_1 < \alpha_2 < \ldots < \alpha_k < \ldots$ of the Sturm-Liouville problem (65), and the corresponding eigenfunctions $\Phi_k(y)$ are orthogonal with respect to the weight function $a_2(y)$,

$$\int_0^1 a_2(y)\Phi_k(y)\Phi_l(y)dy = \delta_{kl}. \tag{66}$$

Denoting by $R_{1,\alpha}(x)$ the solution of

$$(a_1(x)R_{1,\alpha}'(x))' - (\alpha a_1(x) + c_1\eta_1(x))R_{1,\alpha}(x) = 0, \quad R_{1,\alpha}(-\underline{c}) = 0, R_{1,\alpha}(L) = 1,$$

and by $R_{2,\alpha}(x)$ the solution of

$$(a_1(x)R_{2,\alpha}^{'}(x))^{'} - (\alpha a_1(x) + c_1\eta_1(x))R_{2,\alpha}(x) = 0, \quad R_{1,\alpha}(0) = 1, R_{1,\alpha}(\bar{d}) = 0,$$

the subdomain solutions are of the form $u_i^n(x,y) = \sum_\alpha A_{i,\alpha}^n R_{i,\alpha}(x)\Phi_\alpha(y)$, and we use this to decouple the transmission conditions (63) and (64). When $\mathcal{S}_1 = pa_1(L)a_2(y)$, we obtain using the orthogonality property (66) that (63) becomes

$$A_{1,\alpha_i}^n(R_{1,\alpha_i}^{'} + pR_{1,\alpha_i})(L) = A_{2,\alpha_i}^{n-1}(R_{2,\alpha_i}^{n-1} + pR_{2,\alpha_i})(L), \quad \text{for } i = 1,2,\ldots.$$

In a similar fashion, we obtain

$$A_{2,\alpha_i}^n(R_{2,\alpha_i}^{'} - pR_{1,\alpha_i})(0) = A_{1,\alpha_i}^{n-1}(R_{1,\alpha_i}^{'} - pR_{1,\alpha_i})(0), \quad \text{for } i = 1,2,\ldots.$$

We therefore obtain for the convergence factor

$$\rho = \frac{R_{2,\alpha}^{'}(L) + pR_{2,\alpha}(L)}{R_{1,\alpha}^{'}(L) + pR_{1,\alpha}(L)} \frac{R_{1,\alpha}^{'}(0) - pR_{1,\alpha}(0)}{R_{2,\alpha}^{'}(0) - pR_{2,\alpha}(0)}.$$

To optimize this convergence factor, one needs results similar to those described in Lemmas 5 and 6, which can be proved in a similar fashion as for the elliptical domain decomposition. Then, the optimized transmission parameter p^* follows.

Note that we only considered Robin transmission conditions, but other transmission conditions can be analyzed similarly, including the case where a second order differential operator along the interface is used. If in the model problem (61) the coefficients are more general than described by (62), it is not possible to use the technique of separation of variables any more, but then one could derive approximations by using a variable separated approximation to the coefficients.

5 Numerical experiments

We now perform some numerical experiments to illustrate our analysis. We consider the model problem (1) in the domain

$$\Omega = \{(x,y)|x = f\cosh\xi\cos\theta, y = f\sinh\xi\sin\theta, 0 \le \xi < \bar{\Xi}, 0 \le \theta < 2\pi\}$$

with a homogeneous Dirichlet boundary condition on the boundary $\partial\Omega$, and we assume that $f = 1$ and $\bar{\Xi}$ is positive. We solve the model problem (1) with parameter $\eta = 2$ using the parallel Schwarz algorithm (5)-(6) with the domain decomposition $\bar{\Omega} = \bar{\Omega}_1 \cup \bar{\Omega}_2$,

$$\Omega_1 = \{(x,y)|x = f\cosh\xi\cos\theta, y = f\sinh\xi\sin\theta, 0 \le \xi < \Xi + L, 0 \le \theta < 2\pi\},$$
$$\Omega_2 = \{(x,y)|x = f\cosh\xi\cos\theta, y = f\sinh\xi\sin\theta, \Xi \le \xi < \bar{\Xi}, 0 \le \theta < 2\pi\},$$

where Ξ is a subdomain geometry parameter satisfying $0 < \Xi < \bar{\Xi}$ and $L \ge 0$ is the overlap. We discretize the problem using linear finite elements,

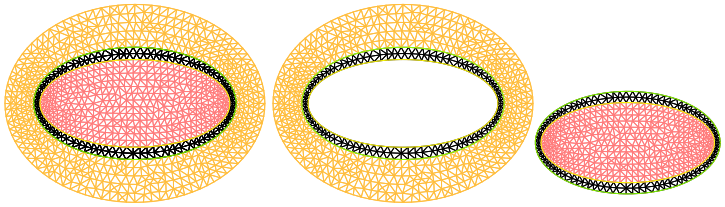

Fig. 6 Mesh used in the numerical experiments for $h = \frac{1}{8}$: on the left the discretization of the entire domain Ω, in the middle the subdomain Ω_1 and on the right the subdomain Ω_2.

and implement the optimized Schwarz methods using FreeFem++ [32] for the homogeneous case $g = 0$, which is equivalent to simulate directly the error equations. The mesh we used is shown in Figure 6, where the number of nodes on the interface is given by the integer part of the ratio of the interface length over h with h being the mesh parameter. For the overlapping case, we set the overlap to $L = h$. In Figure 6 we can see that an adaptive mesh is automatically generated by FreeFem++. We start the error iteration with a random initial guess, which is important for testing, see [17, Figure 5.2], and we show the number of iterations required to reduce the relative error by a factor of $1e-6$. We test two cases : Ξ relatively large, which means a fairly round ellipse, and Ξ relatively small, which means a quite flat and elongated ellipse. Since the optimality of the predicted transmission parameters were extensively numerically tested in [16,24,28,26], we focus on comparing the strategies S1, S2, S3 and S4 discussed in subsection 4. In our setting, we have $\bar{q} = \frac{1}{2}$ and the smallest eigenvalue $\alpha_{\min}$ of the Sturm-Liouville problem (11) is determined by the smallest even mode, i.e. $\alpha_{\min} = \alpha_0^e \approx -0.1218$, which one can compute with the Maple command $MathieuA(0, \bar{q})$.

For fairly round ellipses as interfaces, we fix the parameters $\bar{\Xi} := 1$ and $\Xi := 0.5$, which results in a finite domain Ω that is decomposed into two subdomains with fairly round ellipses as interfaces. Using the strategies S1, S2 and S3, we obtain $G_{\min}^{S1} = 2.7797$, $G_{\min}^{S2} = 2.7783$ and $G_{\min}^{S3} = 2.3843$, where we used a superscript to indicate the way the value $G_{\min}$ is estimated. Since these three values are close (the first two values are almost the same), we can expect that they lead to similar performance of the optimized Schwarz methods. This is confirmed by Table 1 on the left, where we see that the OSMs with $G_{\min}$ estimated by each strategy performs the same, and the results satisfy the asymptotic convergence rate estimates.

To obtain quite flat and elongated ellipses as interfaces, we keep $\bar{q} = 1/2$, but choose now $\Xi = 0.05$ and $\bar{\Xi} = 0.1$. Using the strategies S1, S2 and S3, we find that $G_{\min}^{S1} = 20.0587$, $G_{\min}^{S2} = 20.4587$ and $G_{\min}^{S3} = 1.8796$, which is quite different from the other two. The numerical results are shown in Table 1 (right). As expected, the OSMs with $G_{\min}$ estimated by strategies S1 and S2 perform the same; the performance of S3 differs, but again each optimized

Table 1 Number of iterations required by overlapping and in parenthesis nonoverlapping OSMs with different transmission conditions, for fairly round elliptical domains with $\Xi = 0.5$ (left) and quite flat and elongated elliptical domains with $\Xi = 0.05$ (right).

	h	$\frac{1}{16}$	$\frac{1}{32}$	$\frac{1}{64}$	$\frac{1}{128}$	$\frac{1}{64}$	$\frac{1}{128}$	$\frac{1}{256}$	$\frac{1}{512}$
	S1	6(27)	7(36)	9(54)	12(75)	10(21)	6(29)	8(41)	9(58)
OO0	S2	6(27)	7(36)	9(54)	12(75)	10(21)	6(29)	8(41)	9(58)
	S3	6(25)	7(34)	10(50)	12(70)	46(7)	36(9)	31(12)	22(17)
	S1	6(10)	6(11)	5(13)	6(15)	16(9)	12(10)	10(11)	8(13)
OO2	S2	6(10)	6(11)	5(13)	6(15)	16(9)	12(10)	10(11)	8(13)
	S2	6(10)	6(11)	6(13)	6(16)	69(42)	65(36)	68(31)	55(25)
	S1	5(16)	7(18)	10(23)	12(26)	5(16)	6(19)	9(22)	11(25)
O2s	S2	5(16)	7(18)	10(23)	12(26)	5(16)	6(19)	9(22)	11(25)
	S3	5(15)	7(17)	9(21)	11(24)	14(22)	10(26)	11(31)	13(39)

Table 2 Number of iterations required by the strategy S4 for optimized Schwarz iterations with a fairly round ellipse as interface $\Xi = 0.5$ (left) and a flat ellipse as interface $\bar{\Xi} = 0.05$ (right).

h	$\frac{1}{16}$	$\frac{1}{32}$	$\frac{1}{64}$	$\frac{1}{128}$	$\frac{1}{64}$	$\frac{1}{128}$	$\frac{1}{256}$	$\frac{1}{512}$
OO0	5(23)	7(31)	10(46)	14(64)	27(14)	24(19)	24(27)	23(39)
O2s	9(16)	8(18)	8(23)	9(26)	15(17)	11(23)	11(29)	13(35)

Schwarz method satisfies the asymptotic convergence rate estimate, although we needed to use a finer mesh here to see this. Since $G_{\min}^{S3}$ is very different from $G_{\min}^{S1}$ (which is the numerically calculated best possible value for $G_{\min}$), we would expect that $G_{\min}^{S3}$ performs much worse than $G_{\min}$ estimated by the strategies S1 and S2. This is also true, except in one case, namely with the OO0 transmission condition, where S3 outperforms the other two, which can not be explained by our analysis and needs further investigation.

We finally test strategy S4 which differs from the other three since it does not require the calculation of the smallest eigenvalue $\alpha_{\min}$. In Table 2 we show on the left the results for fairly round ellipses, $\Xi = 0.5$, and on the right the results for flat and elongated ellipses, $\Xi = 0.5$. We do not consider the OO2 transmission condition, since in our case the OO2 transmission condition differs from the one proposed in [16] and thus cannot be approximated by Strategy S4. We see that the strategy S4 leads to acceptable performance of the OSMs: when the interface is fairly round, the strategy S4 performs similarly as the strategies S1, S2 and S3, which is quite exciting. When the interface ellipse becomes however more flat, the strategy S4 deteriorates: it requires much more iterations than the strategies S1 and S2 and also need a more refined mesh to reach the asymptotic regime. Again, the nonoverlapping OSM with OO0 transmission condition is an exception, where S4 outperforms S1.

6 Conclusion

We presented a rigorous analysis of OSMs with elliptical domain decompositions and derived several classes of optimized transmission conditions and

their corresponding asymptotic convergence rate estimates. Our analysis is based on transforming the model problem using elliptic coordinates into a problem with variable reaction term, separation of variables, and a detailed analysis of the monotonicity properties of the ratio of the derivative of radial Mathieu like functions and the Mathieu like function itself. We discovered a key factor, namely $G_{\min}$, which contains the domain geometry for OSMs, and allows us to obtain a unified formula for the optimized transmission parameters and the corresponding convergence rate estimates. We also proposed a new technique for calculating $G_{\min}$, based on the observation that the factor $G_{\min}$ occurs in the classical Schwarz method. It is therefore possible to avoid complicated derivative calculations of Mathieu like functions, and numerically we find that the new approach leads to the same performance. In addition, our analysis suggests that, for irregular domain decompositions, one can formally use our proposed unified formulas of the optimized transmission parameters with $G_{\min}$ estimated by considering the domain geometries. We also showed that our approach can be used to analyze OSMs for more general, variable coefficient problems. In particular, our ideas can be used to analyze OSMs for Helmholtz problems with elliptical domain decompositions as well; however, since there are essential differences between the Helmholtz problem and our model problem here, especially for the case of large wave numbers, our results cannot directly be applied and further analysis would be needed.

References

1. W. O. Amrein, A. M. Hinz, and D. B. Pearson. *Sturm-Liouville Theory: Past and Present*. Birkhäuser Verlag, 2005.
2. M. Baeva, P. Baev, and A. Kaplan. An analysis of the heat transfer from a moving elliptical cylinder. *Journal of Physics D: Applied Physics*, 30(8):1190, 1997.
3. M. Bakker. Modeling groundwater flow to elliptical lakes and through multi-aquifer elliptical inhomogeneities. *Advances in Water Resources*, 27(5):497 – 506, 2004.
4. M. Bakker and K. L. Kuhlman. Computational issues and applications of line-elements to model subsurface flow governed by the modified Helmholtz equation. *Advances in Water Resources*, 34(9):1186 – 1194, 2011.
5. D. Bennequin, M. J. Gander, L. Gouarin, and L. Halpern. Optimized Schwarz waveform relaxation for advection reaction diffusion equations in two dimensions. *Numerische Mathematik*, 134(3):513–567, 2016.
6. D. Bennequin, M. J. Gander, and L. Halpern. A homographic best approximation problem with application to optimized Schwarz waveform relaxation. *Mathematics of Computation*, 78(265):185–223, 2009.
7. M. El Bouajaji, V. Dolean, M. J. Gander, and S. Lanteri. Optimized Schwarz methods for the time-harmonic Maxwell equations with damping. *SIAM Journal on Scientific Computing*, 34(4):A2048–A2071, 2012.
8. Chris Brimacombe, Robert M. Corless, and Mair Zamir. Computation and applications of Mathieu functions: A historical perspective. *arXiv preprint arXiv:2008.01812*, 2020.
9. S. A. Chaplygin. *New methods in the approximate integration of differential equations (in Russian)*. Gostiekhizdat, Moscowa, 1950.
10. G. Ciaramella and M. J. Gander. Analysis of the parallel Schwarz method for growing chains of fixed-sized subdomains: Part II. *SIAM Journal on Numerical Analysis*, 56(3):1498–1524, 2018.
11. G. Ciaramella and M. J. Gander. Analysis of the parallel Schwarz method for growing chains of fixed-sized subdomains: Part III. *Electronic Transactions on Numerical Analysis*, 49:201–243, 2018.

12. V. Dolean, M. J. Gander, and L. Gerardo-Giorda. Optimized Schwarz methods for Maxwell's equations. *SIAM Journal on Scientific Computing*, 31(3):2193–2213, 2009.
13. V. Dolean, M. J. Gander, S. Lanteri, J.-F. Lee, and Z. Peng. Effective transmission conditions for domain decomposition methods applied to the time-harmonic curl–curl Maxwell's equations. *Journal of Computational Physics*, 280:232–247, 2015.
14. T. B. A. El Bashir. Numerical solution of stokes flow generated by vortices: part 2, inside an elliptical cylinder. *Acta Mechanica*, 224(11):2881–2894, 2013.
15. O. G. Ernst and M. J. Gander. Why it is difficult to solve Helmholtz problems with classical iterative methods. In *Numerical Analysis of Multiscale Problems*, pages 325–363. Springer, 2012.
16. M. J. Gander. Optimized Schwarz methods. *SIAM Journal on Numerical Analysis*, 44(2):699–731, 2006.
17. M. J. Gander. Schwarz methods over the course of time. *Electronic Transactions on Numerical Analysis*, 31(5):228–255, 2008.
18. M. J. Gander. On the influence of geometry on optimized Schwarz methods. *SeMA J.*, 53(1):71–78, 2011.
19. M. J. Gander. Iterative methods for Helmholtz and Maxwell equations. *Mathematisches Forschungsinstitut Oberwolfach, Report*, 55:10–11, 2012.
20. M. J. Gander and L. Halpern. Absorbing boundary conditions for the wave equation and parallel computing. *Mathematics of Computation*, 74(249):153–176, 2005.
21. M. J. Gander and L. Halpern. Optimized Schwarz waveform relaxation methods for advection reaction diffusion problems. *SIAM Journal on Numerical Analysis*, 45(2):666–697, 2007.
22. M. J. Gander, L. Halpern, and F. Magoulès. An optimized Schwarz method with two-sided Robin transmission conditions for the Helmholtz equation. *International Journal for Numerical Methods in Fluids*, 55(2):163–175, 2007.
23. M. J. Gander, L. Halpern, and F. Nataf. Optimal Schwarz waveform relaxation for the one dimensional wave equation. *SIAM Journal on Numerical Analysis*, 41(5):1643–1681, 2003.
24. M. J. Gander and Y. Xu. Optimized Schwarz methods for circular domain decompositions with overlap. *SIAM Journal on Numerical Analysis*, 52(4):1981–2004, 2014.
25. M. J. Gander and Y. Xu. Optimized Schwarz method with two-sided transmission conditions in an unsymmetric domain decomposition. In *Domain Decomposition Methods in Science and Engineering XXII*, pages 631–639. 2016.
26. M. J. Gander and Y. Xu. Optimized Schwarz methods for model problems with continuously variable coefficients. *SIAM Journal on Scientific Computing*, 38(5):A2964–A2986, 2016.
27. M. J. Gander and Y. Xu. Optimized Schwarz methods for domain deompositions with parabolic interfaces. In *Domain Decomposition Methods in Science and Engineering XXIII*, pages 323–331. 2017.
28. M. J. Gander and Y. Xu. Optimized Schwarz methods with nonoverlapping circular domain decomposition. *Mathematics of Computation*, 86(304):637–660, 2017.
29. M. J. Gander and H. Zhang. Optimized Schwarz methods with overlap for the Helmholtz equation. *SIAM Journal on Scientific Computing*, 38(5):A3195–A3219, 2016.
30. M. J. Gander and H. Zhang. A class of iterative solvers for the Helmholtz equation: Factorizations, sweeping preconditioners, source transfer, single layer potentials, polarized traces, and optimized Schwarz methods. *SIAM Review*, 2019. in print.
31. J. C. Gutiérrez-Vega. *Formal analysis of the propagation of invariant optical fields in elliptic coordinates*. PhD thesis, INAOE, 2000.
32. F. Hecht. New development in freefem++. *Journal of Numerical Mathematics*, 20(3-4):251–265, 2012.
33. H. von Helmholtz. Theorie der Luftschwingungen in Röhren mit offenen Enden. *Journal für die reine und angewandte Mathematik*, 57:1–72, 1860.
34. C. Japhet, F. Nataf, and F. Rogier. The optimized order 2 method: application to convection–diffusion problems. *Future generation computer systems*, 18(1):17–30, 2001.
35. K. Jiang, X. Han, and K. Ren. Scattering of a gaussian beam by an elliptical cylinder using the vectorial complex ray model. *Journal of the Optical Society of America A*, 30(8):1548–1556, 2013.

36. M. Lai. Fast direct solver for poisson equation in a 2d elliptical domain. *Numerical Methods for Partial Differential Equations*, 20(1):72–81, 2004.
37. A. N. Malyshev. Computation of smallest eigenvalues in the Sturm-Liouville problem with strongly varying coefficients. *SIAM Journal on Matrix Aanalysis and Applications*, 28(4):961–970, 2006.
38. V. Martin. Schwarz waveform relaxation algorithms for the linear viscous equatorial shallow water equations. *SIAM Journal on Scientific Computing*, 31(5):3595–3625, 2009.
39. F. G. Mitri. Acoustic backscattering and radiation force on a rigid elliptical cylinder in plane progressive waves. *Ultrasonics*, 66:27 – 33, 2016.
40. S. A. Patel and R. P. Chhabra. Steady flow of Bingham plastic fluids past an elliptical cylinder. *Journal of Non-Newtonian Fluid Mechanics*, 202:32–53, 2013.
41. S. A. Patel and R. P. Chhabra. Laminar free convection in Bingham plastic fluids from an isothermal elliptic cylinder. *Journal of Thermophysics and Heat Transfer*, 30(1):152–167, 2016.
42. S. A. Patel and R.P. Chhabra. Heat transfer in bingham plastic fluids from a heated elliptical cylinder. *International Journal of Heat and Mass Transfer*, 73:671 – 692, 2014.
43. A. Qaddouri, L. Laayouni, S. Loisel, J. Côté, and M. J. Gander. Optimized Schwarz methods with an overset grid for the shallow-water equations: preliminary results. *Applied Numerical Mathematics*, 58(4):459–471, 2008.
44. A. A. Rodriguez and L. Gerardo-Giorda. New nonoverlapping domain decomposition methods for the harmonic Maxwell system. *SIAM Journal on Scientific Computing*, 28(1):102–122, 2006.
45. M. Sheikholeslami, R. Ellahi, M. Hassan, and S. Soleimani. A study of natural convection heat transfer in a nanofluid filled enclosure with elliptic inner cylinder. *International Journal of Numerical Methods for Heat & Fluid Flow*, 24(8):1906–1927, 2014.
46. J. Shen and L. Wang. On spectral approximations in elliptical geometries using Mathieu functions. *Mathematics of Computation*, 78:815–844, 2009.
47. A. Vion and C. Geuzaine. Double sweep preconditioner for optimized schwarz methods applied to the helmholtz problem. *Journal of Computational Physics*, 266:171–190, 2014.
48. Y. Xu. The influence of domain truncation on the performance of optimized Schwarz methods. *Electronic Transactions on Numerical Analysis*, 49:182–209, 2018.
49. E. Zauderer. *Partial differential equations of applied mathematics*, volume 71. John Wiley & Sons, 2011.